Mechanism and Machine Theory 116 (2017) 326–351

Contents lists available at ScienceDirect

Mechanism and Machine Theory

journal homepage: www.elsevier.com/locate/mechmachtheory

Research paper

Design of six-bar function generators using dual-order structural error and analytical mobility criteria

Saurav Agarwal, Sandipan Bandyopadhyay*

Department of Engineering Design, Indian Institute of Technology Madras, Chennai, Tamil Nadu 600 036, India

ARTICLE INFO

Article history:
Received 25 September 2016
Revised 1 February 2017
Accepted 4 April 2017
Available online 20 June 2017

Keywords:
Six-bar mechanisms
Mobility criteria
Function generation
Double-dwell
Watt-II
Stephenson-III

ABSTRACT

This paper introduces a new approach for the design of planar six-bar mechanisms for the purpose of function generation. The structural error is formulated using the input-output relationship of such a mechanism. In addition to the conventional structural error, its derivative is minimised via numerical optimisation, leading to the novel concept of *dual-order structural error*, which lends itself naturally to a multi-objective formulation of the design problem. Furthermore, analytical conditions for the mobility of the mechanism are derived for two cases: mobility for the full cycle of the crank, and for any given subset of it, along with the identification of the kinematic branches. These conditions help confine the numerical search for the optimal designs to the feasible regions of the design space, leading to a very efficient computational scheme. The results obtained are better in accuracy as compared to the reported results in existing literature. The formulation and results are demonstrated in the context of the Watt-II and the Stephenson-III mechanisms.

1. Introduction

This paper reports new mathematical formulations, which aid the design of planar six-bar mechanisms for the purpose of function generation. In particular, fresh developments are reported with regard to the criteria for the mobility of the Watt-II and the Stephenson-III mechanisms. Also, a new concept, termed hereinafter as the *dual-order structural error*, is introduced. It leads to a multi-objective optimisation formulation for the function generation problem, which, for a number of sample problems studied in the paper, produces results better than those reported in the existing literature, including in the cases where exact synthesis methods were employed.

Traditionally, four-bar mechanisms are used for the purpose of mechanical function generators, following, e.g., the *precision point* approach introduced by Freudenstein [1]. Four-bar mechanisms posses only three independent link ratios (i.e., only three *design variables*), and hence, they can match an arbitrary desired output function *exactly* at three points, at the most. In comparison, the six-bar mechanisms afford much larger design spaces—the three six-bar mechanisms most suitable for function generation, i.e., Stephenson-II, Stephenson-III and Watt-II, have 11 architecture parameters each. Naturally, the six-bar function generators have better potential in terms of accuracy, more so, while approximating highly non-linear functions, which require larger numbers of precision points to describe them accurately over the desired interval of crank motion. This fact was recognised fairly early and there have been sporadic instances of development of such mechanisms as far back as 1940 [2]. However, not many applications and/or theoretical developments have been reported in this regard.

* Corresponding author.
E-mail addresses: agr.saurav1@gmail.com (S. Agarwal), sandipan@iitm.ac.in (S. Bandyopadhyay).

http://dx.doi.org/10.1016/j.mechmachtheory.2017.04.016
0094-114X/

Recently, an *exact* synthesis of six-bar mechanisms for function generation has been carried out using 8 precision points [3]. The resulting equations, if reduced to a *univariate polynomial*, would have had a total degree of 705432, which would have been practically impossible to solve accurately, even if it could be derived. Hence the set of equations were solved using a *homotopy*-based numerical method, implemented in the special purpose software, `Bertini` [4], leading to 92736 *non-singular* and non-degenerate real solutions. In a more recent work [5], the same group of researches have performed an *exact* synthesis of Stephenson-II mechanisms, having 11 precision points. In this case, starting with a potential solution count of 264241152, a total of 1521037 non-singular solutions are obtained, after running on a 256-core 2.2 GHz computer for 311 h. After some additional post processing, 51 usable solutions were found for the case of hip-motion generator. In the case of Stephenson-III mechanisms, the same team track 55050240 initial solutions to obtain 834441 solutions in 40 h, using a 512-core 2.6 GHz computer on this occasion.

While the recent works reported above represent significant landmarks in the field of computational kinematics, they demand colossal computing resources to obtain the mathematically feasible solutions, not to mention the additional efforts required to identify the set of physically realisable mechanisms from this set. Besides, the use of specific mathematical formulations and consequently highly specialised computational tools are warranted in such analysis. Furthermore, in spite of the potentially huge number of candidate solutions considered at the beginning, a very small number of the final solutions are typically found to be *real* and *feasible*. For example, only 51 feasible solutions were obtained for 11 point synthesis in [5]. Finally, though the formulation and the solutions obtained are *exact* in nature (subject only to certain numerical precision involved), the final check for feasibility/mobility is not analytical, but procedural [6].

An alternative approximate approach, namely, numerical optimisation, can be applied to such situations, which is capable of using simpler formulations and more generic computational tools, while producing results which can be constrained *a priori* to satisfy *any* additional requirements. In the case of the four-bar, several such studies have been reported (see, e.g., [7,8]) for the coupler-curve synthesis problem, even after the nine-point coupler-curve synthesis problem was solved exactly in [9]. For the kinematic synthesis of six-bar mechanisms for function generation, however, the authors were not able to trace a single report pertaining to the optimisation approach (except for a preliminary version of the present work, reported in [10]). This observation may be attributed to the fact that the kinematic formulations of either the objectives or the constraint functions for the six-bar mechanisms are not available in reported literature (to the best of the knowledge of the authors). For instance, a function generator would need to be free of singularities, at least in the desired range of the input. It is hard to incorporate such a requirement in the optimisation process, as no generic "Grashof-like" analytical criteria for feasibility exist in the case of the six-bar mechanisms.

These difficulties have not allowed six-bar mechanisms to be used for function generation, up to their full potential. For instance, a particular class of problems, known as the *double-dwell* synthesis, has been solved using six-bar mechanisms of the Stephenson-III type for many years [11–13]. In this problem, the input is a crank, and the output is a rocker, that has to dwell for finite motions of the crank at both the extremities of its excursion. However, the synthesis of this mechanism has been done traditionally via its reduction to a simpler problem—namely, the coupler-curve synthesis of the four-bar mechanism, having two approximately circular arcs of identical radius of curvature [12].

The present work proposes an optimisation approach to the design of the six-bar function generator mechanisms, in particular, the Watt-II and the Stephenson-III mechanisms. It builds upon several new results, related to the partial and full-cycle mobility, such as explicit conditions on the link lengths, which allow the mechanism to be assembled, and be free of singularities. These new developments allow the identification of combinations of design variables leading to feasible mechanisms with accuracy and certainty. Moreover, they involve only the architecture parameters in such calculations (as opposed to the joint variables), leading to fewer computations.

The formulation of the problem in this work starts with the elimination of the unknown joint variables from the *loop-closure* equations, till only the desired output variable remains. Solutions of this scalar univariate equation (termed as the *forward kinematic univariate* or the *FKU* in brief, following [14]) define the kinematic branches of the mechanism. The branches are identified using the singularity functions, which are derived following the analysis of the constraint Jacobian matrices, as shown in [15]. Each branch is studied independently to identify the potential solutions in it, alleviating the branch-error problem as well in the process. The singularity conditions are converted to polynomials in an algebraic variable representing the crank motion. Characterisation of the roots of these polynomials leads to the identification of the *singularity-free* mechanisms. The problem of computation of assembly constraints is also solved similarly, leading to the identification of link geometries capable of assembling into a feasible mechanism, at a nominal computational expense. Finally, the *structural error*, to be minimised in the optimisation process, is defined in a novel manner. The departure of the generated output function, from the desired output function, is treated as the *zeroth-order* error function, which is in accordance with the standard practice. In addition, a *first-order* error function is defined, which is the derivative of the zeroth order error function. The design method tries to reduce *both* the errors simultaneously, and independently, in what may be called a *dual-order* formulation of the design problem. As the latter objective aids the former, the final results obtained are typically better than in the conventional methods, wherein only the zeroth-order structural errors are considered.

For the solution of the problem formulated as above, a Genetic Algorithm (GA)-based optimiser, namely, `NSGA-II` [16], has been used. Such an optimiser is ideally suited for the problem at hand, since it handles multi-objective problems. It also performs a global exploration, and hence, does not require any initial guess. Furthermore, it is relatively insensitive to the dimension of the design space—which, aided by the confinement of the search for optimal designs to only the feasible regions, allows for satisfactory exploration of the design space in a computationally efficient manner. The results obtained prove to

be of very high quality—they are *better* than the results reported in existing literature in all the benchmark problems studied in this paper, in terms of the accuracy, measured in terms of the maximum absolute (zeroth-order) structural error over the designated range of motion. It may be noted, that the said results are obtained at a tiny fraction of the computational expenses warranted by the exact method—typically, in about 10 min, while running four processes simultaneously on a standard desktop computer. The accuracy of the design solutions, their guaranteed adherence to the mobility criteria and additional constraints, and the computational efficiency with which they are achieved, make the proposed design method fairly attractive from the perspective of practical design. From a broader theoretical perspective, the concept of dual-order structural error, and the conditions for mobility over a full cycle of the input or a specified part thereof, constitute the main contributions of this work.

The rest of the paper is organised as follows: the description of the mechanisms and the corresponding kinematic formulations are given in Section 2. The formulation of the mobility criteria, using assembly and singularity conditions, is described in Section 3. The derivation of the mobility conditions over a desired range, and the discussion on identifying branches of the mechanisms is detailed in Section 4. Formalisation of the function generation problem with dual-order objectives is done in Section 5. The numerical studies on several benchmark problems are presented in Section 6. Finally, the conclusions are presented in Section 7.

2. Kinematic formulation

The zeroth and first order position kinematics of the Watt-II and the Stephenson-III mechanisms are derived in this section.

2.1. Kinematics

The single independent (i.e., input/actuated) joint variable is denoted by θ, hereafter. The m dependent (i.e., passive/unactuated) variables are denoted by $\boldsymbol{\phi}$. The dependent variables are related to the independent variables via m scalar *loop-closure* constraint equations, which can be written as:

$$\boldsymbol{\eta}(\theta, \boldsymbol{\phi}) = \mathbf{0}, \;\; \boldsymbol{\phi} \in \mathbb{R}^m. \tag{1}$$

In general, it is possible to eliminate $(m-1)$ passive variables from the loop-closure equations to obtain a univariate equation in the output variable, say, ϕ_m. The coefficients of this equation would be functions of the architecture parameters and the input variable, θ. This univariate equation has been termed as the *forward kinematics univariate* (FKU) [14] equation and can be written as:

$$f(\theta, \phi_m) = 0. \tag{2}$$

In order to obtain the *velocity coefficient* (see, e.g., [13]) of the output variable with respect to the input variable, the FKU, given in Eq. (2), is differentiated with respect to time:

$$\frac{\partial f}{\partial \theta}\dot{\theta} + \frac{\partial f}{\partial \phi_m}\dot{\phi}_m = 0. \tag{3}$$

The velocity coefficient of ϕ_m w.r.t. θ is given by:

$$J_{\phi_m\theta} = \dot{\phi}_m / \dot{\theta}. \tag{4}$$

From Eq. (3):

$$\dot{\phi}_m = -\left(\frac{\partial f}{\partial \theta}\right) \Big/ \left(\frac{\partial f}{\partial \phi_m}\right)\dot{\theta}. \tag{5}$$

Comparing Eqs. (4) with (5), the velocity coefficient is given by:

$$J_{\phi_m\theta} = -\left(\frac{\partial f}{\partial \theta}\right) \Big/ \left(\frac{\partial f}{\partial \phi_m}\right), \tag{6}$$

with the understanding that $\frac{\partial f}{\partial \phi_m} \neq 0$ at a non-singular configuration. The velocity coefficient, $J_{\phi_m\theta}$, is a function of ϕ_m, θ and the architecture parameters of the mechanism.

2.2. Forward kinematics of the Watt-II mechanism

The six-bar mechanism of the type Watt-II is shown in Fig. 1. The input angle, θ_1, is associated with link l_1. The passive joint angles are given by $\boldsymbol{\phi} = (\phi_2, \phi_3, \phi_4, \phi_5)^\top$. The output angle, ϕ_5, is associated with the link l_5. The points $\mathbf{o}_1 = (0,0)^\top$, $\mathbf{o}_2 = (l_0, 0)^\top$ and $\mathbf{o}_3 = (o_{3x}, o_{3y})^\top$ locate the fixed pivots of the mechanism. The link $\mathbf{bo}_2\mathbf{c}$ is ternary in nature and is defined by the lengths l_3 and l_a, and the included angle α. The angles θ_0 and ϕ_0 are constant offsets to the input and output angles,

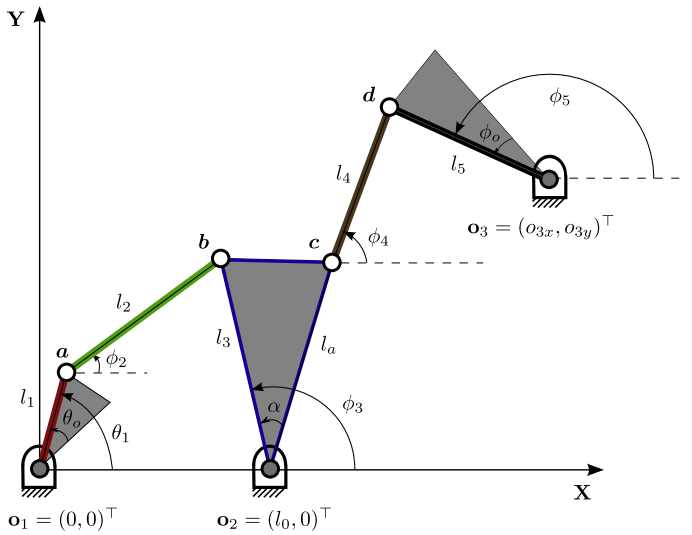

Fig. 1. Schematic of the Watt-II mechanism. The fixed pivots are located at the points $\mathbf{o}_1$, $\mathbf{o}_2$ and $\mathbf{o}_3$. The link $\mathbf{bo}_2\mathbf{c}$ is ternary in nature and is defined by the lengths l_3 and l_a, and the included angle α. The input angle (θ_1) and the output angle (ϕ_5) are associated with the links l_1 and l_5, respectively. The angles θ_0 and ϕ_0 are constant offsets to the input and output angles, respectively.

respectively. The mechanism has 12 architecture parameters, given by $\mathbf{x} = (l_0, l_1, l_2, l_3, l_4, l_5, \alpha, l_a, o_{3x}, o_{3y}, \theta_0, \phi_0)^\top$. For the four-bar loop $\mathbf{o}_1\mathbf{abo}_2\mathbf{o}_1$, the constraint equations can be written as:

$$\eta_1 := l_1 \cos\theta_1 + l_2 \cos\phi_2 - l_0 - l_3 \cos\phi_3 = 0, \tag{7}$$

$$\eta_2 := l_1 \sin\theta_1 + l_2 \sin\phi_2 - l_3 \sin\phi_3 = 0. \tag{8}$$

Similarly, for the other four-bar loop $\mathbf{o}_2\mathbf{cdo}_3\mathbf{o}_2$, the constraint equations can be written as:

$$\eta_3 := l_0 + l_a \cos(\phi_3 - \alpha) + l_4 \cos\phi_4 - o_{3x} - l_5 \cos\phi_5 = 0, \tag{9}$$

$$\eta_4 := l_0 + l_a \sin(\phi_3 - \alpha) + l_4 \sin\phi_4 - o_{3y} - l_5 \sin\phi_5 = 0. \tag{10}$$

The constraint equations, Eqs. (7)–(10), can be compactly written as:

$$\boldsymbol{\eta} := (\eta_1, \eta_2, \eta_3, \eta_4)^\top = \mathbf{0}. \tag{11}$$

The following steps are employed to obtain the FKU from Eq. (11):

- Eqs. (7) and (8) are linear in the sine and the cosine of ϕ_2. Hence, the variable ϕ_2 is eliminated by finding $\cos\phi_2$ and $\sin\phi_2$, and thereafter using the trigonometric identity $\cos^2\phi_k + \sin^2\phi_k = 1$, to obtain the equation:
$$g_1(\theta_1, \phi_3) = 0. \tag{12}$$
- Similarly, the Eqs. (9) and (10) are linear in the sine and the cosine of ϕ_4. The variable ϕ_4 is eliminated as above to obtain the equation:
$$g_2(\phi_3, \phi_5) = 0. \tag{13}$$
- The functions g_1 and g_2, given in Eqs. (12) and (13), respectively, are linear in the sine and the cosine of ϕ_3. The variable ϕ_3 is eliminated to obtain the FKU equation:
$$g_3(\theta_1, \phi_5) = 0. \tag{14}$$
- The function g_3 is converted to a polynomial using the standard tangent half-angle substitution, i.e.:
$$\cos\phi_5 = \frac{1 - t_5^2}{1 + t_5^2} \quad \text{and} \quad \sin\phi_5 = \frac{2t_5}{1 + t_5^2}, \quad \text{where,} \quad t_5 = \tan\frac{\phi_5}{2},$$
to obtain $g_4(\theta_1, t_5) = 0$. The coefficients of the polynomial g_4 are functions of architecture parameters and input angle, θ_1.

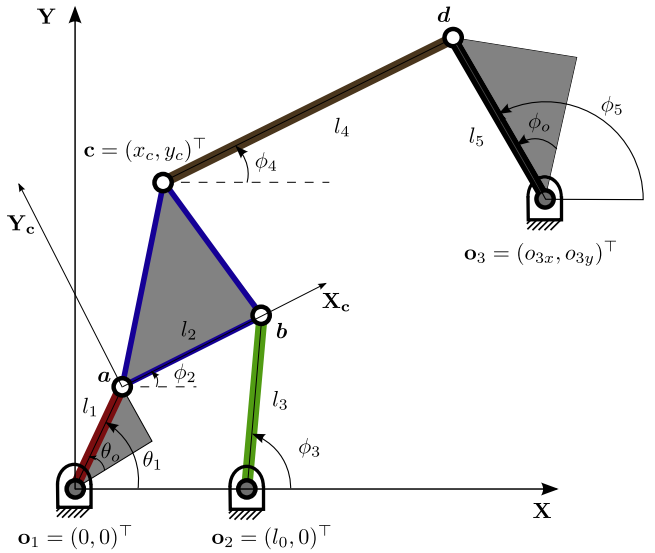

Fig. 2. Schematic of the Stephenson-III mechanism. The fixed pivots are located at the points $\mathbf{o}_1$, $\mathbf{o}_2$ and $\mathbf{o}_3$. The coupler point $\mathbf{c} = (x_c, y_c)^\top$ is specified with respect to the coupler's local reference frame ($\mathbf{X_cY_c}$). The input angle (θ_1) and the output angle (ϕ_5) are associated with the links l_1 and l_5, respectively. The angles θ_0 and ϕ_0 are constant offsets to the input and output angles, respectively.

The derivation of the FKU is summarised in the schematic below:

$$\left.\begin{array}{l}\left.\begin{array}{l}\eta_1(\theta_1,\phi_2,\phi_3)=0\\ \eta_2(\theta_1,\phi_2,\phi_3)=0\end{array}\right)\xrightarrow{\times\phi_2} g_1(\theta_1,\phi_3)=0\\ \left.\begin{array}{l}\eta_3(\phi_3,\phi_4,\phi_5)=0\\ \eta_4(\phi_3,\phi_4,\phi_5)=0\end{array}\right)\xrightarrow{\times\phi_4} g_2(\phi_3,\phi_5)=0\end{array}\right\}\xrightarrow{\times\phi_3} g_3(\theta_1,\phi_5)=0\xrightarrow{\phi_5\to t_5} g_4(\theta_1,t_5)=0. \tag{15}$$

Here, '$\xrightarrow{\times v}$' indicates the elimination of the variable v from two equations in v. The transformation of the trigonometric functions of an angle to their respective tangent half-angle forms is denoted by '$\xrightarrow{\alpha\to t}$' etc., where $t = \tan\frac{\alpha}{2}$.

2.3. Forward kinematics of the Stephenson-III mechanism

The schematic of the six-bar mechanism of the type Stephenson-III is shown in Fig. 2. The input angle, θ_1, is associated with link l_1. The passive joint angles are $\boldsymbol{\phi} = (\phi_2, \phi_3, \phi_4, \phi_5)^\top$. The output angle ϕ_5 is associated with the link l_5. The points $\mathbf{o}_1 = (0,0)^\top$, $\mathbf{o}_2 = (l_0, 0)^\top$ and $\mathbf{o}_3 = (o_{3x}, o_{3y})^\top$ locate the fixed pivots of the mechanism. Point $\boldsymbol{c}$ is the coupler point and its coordinates in the local frame, $\mathbf{X_cY_c}$, of the coupler link, are given by $(x_c, y_c)^\top$. The angles θ_0 and ϕ_0 are constant offsets to the input and output angles, respectively.

For the four-bar loop $\mathbf{o_1abo_2o_1}$, the loop-closure equations can be written as:

$$\eta_1 := l_1\cos\theta_1 + l_2\cos\phi_2 - l_0 - l_3\cos\phi_3 = 0, \tag{16}$$

$$\eta_2 := l_1\sin\theta_1 + l_2\sin\phi_2 - l_3\sin\phi_3 = 0. \tag{17}$$

Similarly, for the five-bar loop $\mathbf{o_1acdo_3o_1}$, the constraint equations can be written as:

$$\eta_3 := l_1\cos\theta_1 + x_c\cos\phi_2 - y_c\sin\phi_2 + l_4\cos\phi_4 - o_{3x} - l_5\cos\phi_5 = 0, \tag{18}$$

$$\eta_4 := l_1\sin\theta_1 + x_c\sin\phi_2 + y_c\cos\phi_2 + l_4\sin\phi_4 - o_{3y} - l_5\sin\phi_5 = 0. \tag{19}$$

The constraint equations, Eqs. (16)–(19), can be compactly written as:

$$\boldsymbol{\eta} := (\eta_1, \eta_2, \eta_3, \eta_4)^\top = \mathbf{0}. \tag{20}$$

Following the elimination procedure similar to that described for the Watt-II mechanism in Section 2.2, the FKU is obtained in terms of the input angle, θ_1, and the output angle, ϕ_5. For the sake of brevity, only the summary of the derivation is presented in the following schematic.

$$\left.\begin{array}{l}\left.\begin{array}{l}\eta_1(\theta_1,\phi_2,\phi_3)=0\\ \eta_2(\theta_1,\phi_2,\phi_3)=0\end{array}\right)\xrightarrow{\times\phi_3} g_1(\theta_1,\phi_2)=0\\ \left.\begin{array}{l}\eta_3(\theta_1,\phi_2,\phi_4,\phi_5)=0\\ \eta_4(\theta_1,\phi_2,\phi_4,\phi_5)=0\end{array}\right)\xrightarrow{\times\phi_4} g_2(\theta_1,\phi_2,\phi_5)=0\end{array}\right\}\xrightarrow{\times\phi_2} g_3(\theta_1,\phi_5)=0\xrightarrow{\phi_5\to t_5} g_4(\theta_1,t_5)=0. \tag{21}$$

2.4. First order kinematics of the Watt-II and the Stephenson-III mechanisms

The velocity coefficient of the output link, l_5, of the Watt-II mechanism is obtained using Eqs. (6) and (14):

$$J_{\phi_5\theta_1}=-\left(\frac{\partial g_3}{\partial\theta_1}\right)\Big/\left(\frac{\partial g_3}{\partial\phi_5}\right). \tag{22}$$

The velocity coefficient, $J_{\phi_5\theta_1}$, is a function of the architecture parameters and the input angle, θ_1.

The velocity coefficient for the output link, l_5, of the Stephenson-III mechanism, is obtained in a similar manner.

3. Formulation of the mobility criteria

While using a numerical optimisation algorithm for design, ranges for each of the design variables, i.e., the architecture parameters, have to be specified. The union of these ranges form the *design space* to be scanned by the optimiser. Not all points in the design space form a mechanically feasible mechanism. Hence, it is important to reject such designs outright without considering them in further computation. Often, one criterion for mechanical feasibility is the *full-cycle mobility*, such that a rotary actuator can be used, without any constraint on the range of the input angle.

A mechanism is said to possess full-cycle mobility if: (1) assembly of the mechanism is possible for the given architecture parameters, and (2) there is no singularity, for a complete rotation of the crank. Analysis of the loop-closure equations can lead to specific conditions, e.g., Grashof's condition (see, e.g., [17]) in the case of the four-bar mechanism. Similar analysis is carried out in the following, for the six-bar mechanisms of the Watt-II and the Stephenson-III types.

3.1. Mobility criteria for the Watt-II mechanism

The four-bar loop $\mathbf{o}_1\mathbf{abo}_2\mathbf{o}_1$ can be assembled *iff* $\forall\theta_1\in\mathbb{R}$, the distance $\overline{\mathbf{ao}_2}\in[|l_2-l_3|,l_2+l_3]$ (see Fig. 3), leading to the conditions:

$$(l_1\cos\theta_1-l_0)^2+(l_1\sin\theta_1)^2\geq(l_2-l_3)^2, \tag{23}$$

$$(l_1\cos\theta_1-l_0)^2+(l_1\sin\theta_1)^2\leq(l_2+l_3)^2. \tag{24}$$

Upon simplification and the use of *slack variables* ϵ_1 and ϵ_2, these inequalities are converted to equations as:

$$\mathcal{F}_1:=-l_0^2-l_1^2+2l_0l_1\cos\theta_1+(l_2-l_3)^2+\epsilon_1=0,\quad \epsilon_1\geq 0; \tag{25}$$

$$\mathcal{F}_2:=\quad l_0^2+l_1^2-2l_0l_1\cos\theta_1-(l_2+l_3)^2+\epsilon_2=0,\quad \epsilon_2\geq 0. \tag{26}$$

The second four-bar loop $\mathbf{o}_2\mathbf{cdo}_3\mathbf{o}_2$ can be assembled *iff* $\forall\theta_1\in\mathbb{R}$, the distance $\overline{\boldsymbol{co}_3}\in[|l_4-l_5|,l_4+l_5]$:

$$(l_0+l_a\cos(\phi_3-\alpha)-o_{3x})^2+(l_a\sin(\phi_3-\alpha)-o_{3y})^2\geq(l_4-l_5)^2, \tag{27}$$

$$(l_0+l_a\cos(\phi_3-\alpha)-o_{3x})^2+(l_a\sin(\phi_3-\alpha)-o_{3y})^2\leq(l_4+l_5)^2. \tag{28}$$

Upon simplification and the use of slack variables ϵ_3 and ϵ_4, these inequalities are converted to equations as:

$$\mathcal{F}_3:=2l_a(l_0-o_{3x})\cos(\alpha-\phi_3)+(l_0-o_{3x})^2+l_a^2+2l_ao_{3y}\sin(\alpha-\phi_3)+o_{3y}^2-(l_4-l_5)^2-\epsilon_3=0,\quad \epsilon_3\geq 0; \tag{29}$$

$$\mathcal{F}_4:=2l_a(l_0-o_{3x})\cos(\alpha-\phi_3)+(l_0-o_{3x})^2+l_a^2+2l_ao_{3y}\sin(\alpha-\phi_3)+o_{3y}^2-(l_4+l_5)^2+\epsilon_4=0,\quad \epsilon_4\geq 0. \tag{30}$$

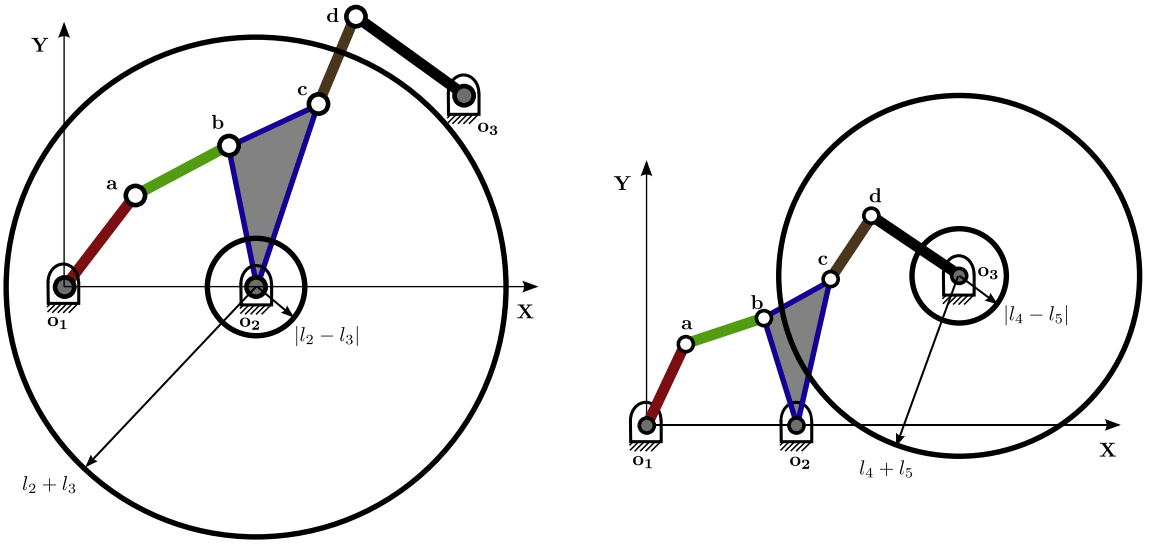

(a) The two concentric circles, centred at $\mathbf{o}_2$ and of radii $l_2 + l_3$ and $|l_2 - l_3|$, respectively, define the boundaries for the feasible region of the first four-bar loop. The point $\mathbf{a}$ lies inside the annulus formed by the two circles.

(b) The two concentric circles, centred at $\mathbf{o}_3$ and of radii $l_4 + l_5$ and $|l_4 - l_5|$, respectively, define the boundaries for the feasible region of the second four-bar loop. The point $\mathbf{c}$ lies inside the annulus formed by the two circles.

Fig. 3. The geometric representation of the assembly conditions of the Watt-II mechanism.

The slack variables $\epsilon_i,\ i = 1, \ldots, 4$, are termed as the *mobility margins*. For the mechanism to be feasible, or in other words, for it to be assembled, the mobility margins should always be positive. The feasibility conditions given in Eqs. (25), (26), (29) and (30) have been represented geometrically in Fig. 3. The annular region—bounded by two concentric circles centred at $\mathbf{o}_3$ and of radii $|l_4 - l_5|$ and $l_4 + l_5$, respectively—define the permissible locations of the point $\mathbf{c}$.

Singularity of a mechanism can be studied via the degeneracy of the Jacobian matrix of the constraint equations with respect to the passive variables [15]. Finding the partial derivatives of the loop-closure equations, $\boldsymbol{\eta}$ (given in Eq. (11)), with respect to $\boldsymbol{\phi}$ gives the constraint Jacobian matrix:

$$\mathbf{J}_{\eta\phi} = \frac{\partial \boldsymbol{\eta}}{\partial \boldsymbol{\phi}}. \tag{31}$$

Singularity occurs when the determinant of $\mathbf{J}_{\eta\phi}$ is zero, where:

$$\det(\mathbf{J}_{\eta\phi}) = l_2 l_3 l_4 l_5 \sin(\phi_2 - \phi_3) \sin(\phi_4 - \phi_5). \tag{32}$$

As the link-lengths need to be non-zero for the mechanism to exist, Eq. (32) factors into two distinct singularity functions, s_1 and s_2:

$$s_1 := \sin(\phi_2 - \phi_3), \tag{33}$$

$$s_2 := \sin(\phi_4 - \phi_5), \quad \text{and} \tag{34}$$

$$s_1 = 0 \Rightarrow \phi_3 = \phi_2, \ \text{or } \phi_2 - \pi, \ \text{considering } \phi_2 - \phi_3 \in [0, 2\pi]. \tag{35}$$

$$s_2 = 0 \Rightarrow \phi_5 = \phi_4, \ \text{or } \phi_4 - \pi, \ \text{considering } \phi_4 - \phi_5 \in [0, 2\pi] \tag{36}$$

The signs of the singularity functions identify the kinematic branches of the mechanism *uniquely*, as shown in Fig. 4:

a) Branch UU, if $s_1 < 0$ and $s_2 < 0$;
b) Branch UD, if $s_1 < 0$ and $s_2 > 0$;
c) Branch DU, if $s_1 > 0$ and $s_2 < 0$;
d) Branch DD, if $s_1 > 0$ and $s_2 > 0$.

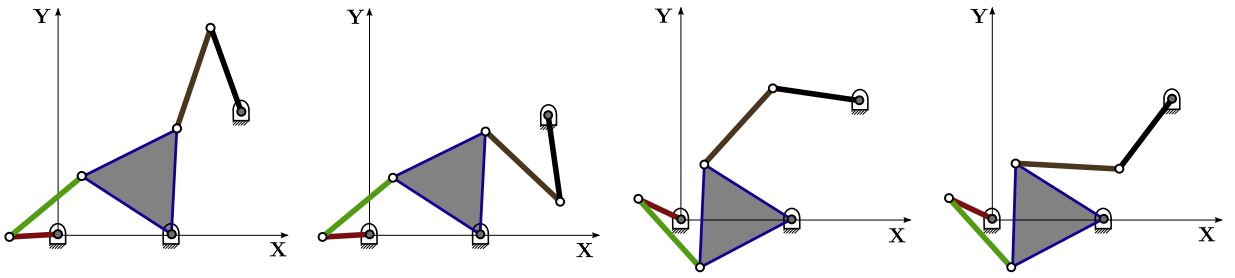

(a) UU: $s_1 < 0,\ s_2 < 0$ (b) UD: $s_1 < 0,\ s_2 > 0$ (c) DU: $s_1 > 0,\ s_2 < 0$ (d) DD: $s_1 > 0,\ s_2 > 0$

Fig. 4. The four branches of the Watt-II mechanism.

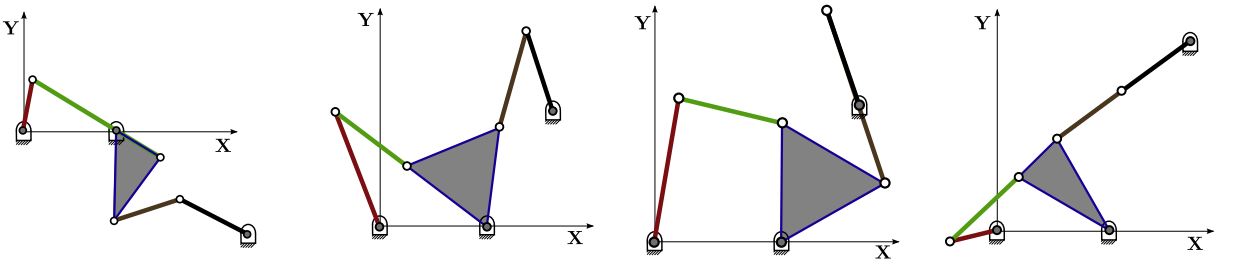

(a) Singularity in four-bar loop: $\phi_3 = \phi_2,\ \mathcal{S}_1 = 0$ (b) Singularity in four-bar loop: $\phi_3 = \phi_2 - \pi,\ \mathcal{S}_2 = 0$ (c) Singularity in RR chain: $\phi_5 = \phi_4,\ \mathcal{S}_3 = 0$ (d) Singularity in RR chain: $\phi_5 = \phi_4 - \pi,\ \mathcal{S}_4 = 0$

Fig. 5. The geometric representation of the four singularity conditions of the Watt-II mechanism. These conditions are mathematically equivalent to vanishing of the singularity functions $\mathcal{S}_1$, $\mathcal{S}_2$, $\mathcal{S}_3$ and $\mathcal{S}_4$, respectively.

Here, the first and the second letters in the branch name denote the configurations of the chains $\mathbf{abo}_2$ and $\mathbf{cdo}_3$, respectively: 'U' denotes *elbow up* and 'D' denotes *elbow down* configurations.

The singularity function given by s_1 in Eq. (33) represents the singularity in the four-bar loop $\mathbf{o}_1\mathbf{abo}_2\mathbf{o}_1$. Singularity occurs when $\phi_3 = \phi_2$, or $\phi_2 - \pi$, i.e., links l_2 and l_3 become collinear. These conditions are depicted in Fig. 5(a) and (b), respectively.

In order to obtain the singularity conditions in terms of the architecture parameters, ϕ_3 is eliminated from Eqs. (7) and (8) by directly using Eq. (35) in the loop-closure equations, thereby leading to two different sets of equations:

(a) $\phi_3 = \phi_2 \Rightarrow \mathbf{e}_1(\theta_1, \phi_2) = (e_{11}, e_{12})^\top = \mathbf{0}$,
(b) $\phi_3 = \phi_2 - \pi \Rightarrow \mathbf{e}_2(\theta_1, \phi_2) = (e_{21}, e_{22})^\top = \mathbf{0}$.

Treating these singularity-specific loop-closure equations in the same way as described in Section 2.1, a non-linear equation is derived, having the input variable θ_1 as the only unknown. The sequential elimination of ϕ_2 and ϕ_3 can be schematically represented as follows:

$$\begin{aligned}
&\left.\begin{aligned}\eta_1(\theta_1,\phi_2,\phi_3) &= 0\\ \eta_2(\theta_1,\phi_2,\phi_3) &= 0\end{aligned}\right\} \xrightarrow{\phi_3=\phi_2} \left.\begin{aligned}e_{11}(\theta_1,\phi_2) &= 0\\ e_{12}(\theta_1,\phi_2) &= 0\end{aligned}\right\} \xrightarrow{\times\phi_2} \mathcal{S}_1(\theta_1) = 0;\\
&\left.\begin{aligned}\eta_1(\theta_1,\phi_2,\phi_3) &= 0\\ \eta_2(\theta_1,\phi_2,\phi_3) &= 0\end{aligned}\right\} \xrightarrow{\phi_3=\phi_2-\pi} \left.\begin{aligned}e_{21}(\theta_1,\phi_2) &= 0\\ e_{22}(\theta_1,\phi_2) &= 0\end{aligned}\right\} \xrightarrow{\times\phi_2} \mathcal{S}_2(\theta_1) = 0.
\end{aligned} \tag{37}$$

The singularity in the loop $\mathbf{o}_2\mathbf{cdo}_3\mathbf{o}_2$ is governed by the function s_2, given in Eq. (34), and occurs when $\phi_5 = \phi_4$, or $\phi_4 - \pi$. This is geometrically equivalent to l_4 and l_5 being collinear, as depicted in Fig. 5(c) and (d), respectively. Following the same steps used in deriving $\mathcal{S}_1$ and $\mathcal{S}_2$, ϕ_5 is eliminated from the loop-closure equations, Eqs. (9) and (10), to obtain a special set of constraint equations, describing the singular configurations:

(a) $\phi_5 = \phi_4 \Rightarrow \mathbf{e}_3(\phi_3, \phi_4) = (e_{31}, e_{32})^\top = \mathbf{0}$;
(b) $\phi_5 = \phi_4 - \pi \Rightarrow \mathbf{e}_4(\phi_3, \phi_4) = (e_{41}, e_{42})^\top = \mathbf{0}$.

The sequential elimination of ϕ_4 and ϕ_5 can be schematically represented as follows:

$$\left.\begin{matrix}\eta_3(\phi_3,\phi_4,\phi_5)=0\\ \eta_4(\phi_3,\phi_4,\phi_5)=0\end{matrix}\right) \xrightarrow{\phi_5=\phi_4} \left.\begin{matrix}e_{31}(\phi_3,\phi_4)=0\\ e_{32}(\phi_3,\phi_4)=0\end{matrix}\right) \xrightarrow{\times\phi_4} \mathcal{S}_3(\phi_3)=0;$$
$$\left.\begin{matrix}\eta_3(\phi_3,\phi_4,\phi_5)=0\\ \eta_4(\phi_3,\phi_4,\phi_5)=0\end{matrix}\right) \xrightarrow{\phi_5=\phi_4-\pi} \left.\begin{matrix}e_{41}(\phi_3,\phi_4)=0\\ e_{42}(\phi_3,\phi_4)=0\end{matrix}\right) \xrightarrow{\times\phi_4} \mathcal{S}_4(\phi_3)=0. \tag{38}$$

The singularity functions $\mathcal{S}_1$ and $\mathcal{S}_2$ in Eq. (37) correspond to the assembly conditions $\mathcal{F}_1$ and $\mathcal{F}_2$ given in Eqs. (25) and (26), when ϵ_1 and ϵ_2 vanish, respectively. Similarly, the singularity functions $\mathcal{S}_3$ and $\mathcal{S}_4$ in Eq. (38) correspond to the assembly conditions $\mathcal{F}_3$ and $\mathcal{F}_4$ given in Eqs. (29) and (30), when ϵ_3 and ϵ_4 fall to zero, respectively. Hence, for the mechanism to possess mobility, i.e., be feasible and non-singular, $\mathcal{F}_i=0$ must hold for some $\epsilon_i>0,\ \ i=1,\ldots,4$.

For further analysis, Eqs. (25) and (26) are converted to their respective polynomial forms by using the tangent-half angle substitution, which are further rearranged to obtain:

$$\epsilon_1(t_1)=t_1^2\left((l_0+l_1)^2-(l_2-l_3)^2\right)+(l_0-l_1)^2-(l_2-l_3)^2 \quad \text{and,} \tag{39}$$

$$\epsilon_2(t_1)=t_1^2\left((l_2+l_3)^2-(l_0+l_1)^2\right)-(l_0-l_1)^2+(l_2+l_3)^2, \ \text{where} \quad t_1=\tan\frac{\theta_1}{2}. \tag{40}$$

Further, recall that a quadratic polynomial with real coefficients, say, $u_0t_1^2+u_1t_1+u_2$, is positive for all real values of t_1 if the leading coefficient, u_0, is positive and the discriminant, $u_1^2-4u_0u_2$, is negative. For $\epsilon_1,\epsilon_2>0\forall t_1\in\mathbb{R}$, the following conditions are hence, derived from Eqs. (39) and (40), respectively:

$$\mathcal{M}_1:=\begin{cases}\mathcal{M}_{1a}:=l_0+l_1+l_3-l_2 & >0,\\ \mathcal{M}_{1b}:=l_0+l_1+l_2-l_3 & >0,\\ \mathcal{M}_{1c}:=(l_0-l_1)^2-(l_2-l_3)^2 & >0;\end{cases} \tag{41}$$

$$\mathcal{M}_2:=\begin{cases}\mathcal{M}_{2a}:=l_1+l_2+l_3-l_0 & >0,\\ \mathcal{M}_{2b}:=l_0+l_2+l_3-l_1 & >0,\\ \mathcal{M}_{2c}:=(l_2+l_3)^2-(l_0+l_1)^2 & >0.\end{cases} \tag{42}$$

The mobility functions, $\mathcal{M}_1$ and $\mathcal{M}_2$, depend only on the link lengths, and hence, represent the characteristics of the mechanism's architecture—and not of a particular configuration. It is required that the values of these functions are greater than zero in a non-singular feasible mechanism. These lead to (an equivalent of) the Grashof's condition (see, e.g., [17]), as expected, for the four-bar loop of the mechanism.

Similarly, the Eqs. (29) and (30) can be converted to their polynomial forms using the function $g_1(\theta_1,\phi_3)$ appearing in Eq. (12) and tangent half-angle substitution:

$$\left.\begin{matrix}\mathcal{F}_3(\phi_3,\epsilon_3)=0\\ g_1(\theta_1,\phi_3)=0\end{matrix}\right) \xrightarrow{\times\phi_3} h_1(\theta_1,\epsilon_3)=0 \xrightarrow{\theta_1\to t_1} h_3(t_1,\epsilon_3)=0;$$
$$\left.\begin{matrix}\mathcal{F}_4(\phi_3,\epsilon_4)=0\\ g_1(\theta_1,\phi_3)=0\end{matrix}\right) \xrightarrow{\times\phi_3} h_2(\theta_1,\epsilon_4)=0 \xrightarrow{\theta_1\to t_1} h_4(t_1,\epsilon_4)=0. \tag{43}$$

The functions h_3 and h_4 are quadratic in ϵ_i: $h_i=A_i(t_1)\epsilon_i^2+B_i(t_1)\epsilon_i+C_i(t_1),\ \ i=3,4$. As ϵ_i are assumed to be positive, the roots of the equations, $h_i=0$, should be real and positive. The leading coefficients, $A_i(t_1)$, are found to be always positive, and hence, the conditions for the quadratics to have positive real roots can be stated as:

$$\begin{aligned}&f_{ia}(t_1)=-B_i(t_1)>0,\\ &f_{ib}(t_1)=C_i(t_1)>0,\\ &f_{ic}(t_1)=B_i^2(t_1)-4A_i(t_1)C_i(t_1)\geq 0,\ \ i=3,4.\end{aligned} \tag{44}$$

The three inequalities, given by Eq. (44), are functions of t_1 and the architecture parameters. The polynomials f_{ia}, f_{ib} and f_{ic} are of degree 4, 4 and 8 in t_1, respectively. However, f_{ic} factorises into two quadratics, k_a and k_b, and the square of a quadratic, k_c:

$$f_{ic}=k_ak_bk_c^2. \tag{45}$$

The quadratics k_a and k_b correspond to the mobility conditions $\mathcal{M}_1$ and $\mathcal{M}_2$ given in Eqs. (41) and (42), respectively. Thus, the mobility conditions of the four-bar are retrieved as a subset of the mobility conditions of the six-bar mechanism, as expected. The factor k_c^2 is obviously non-negative. Hence, the function f_{ic} does not impose any additional restrictions.

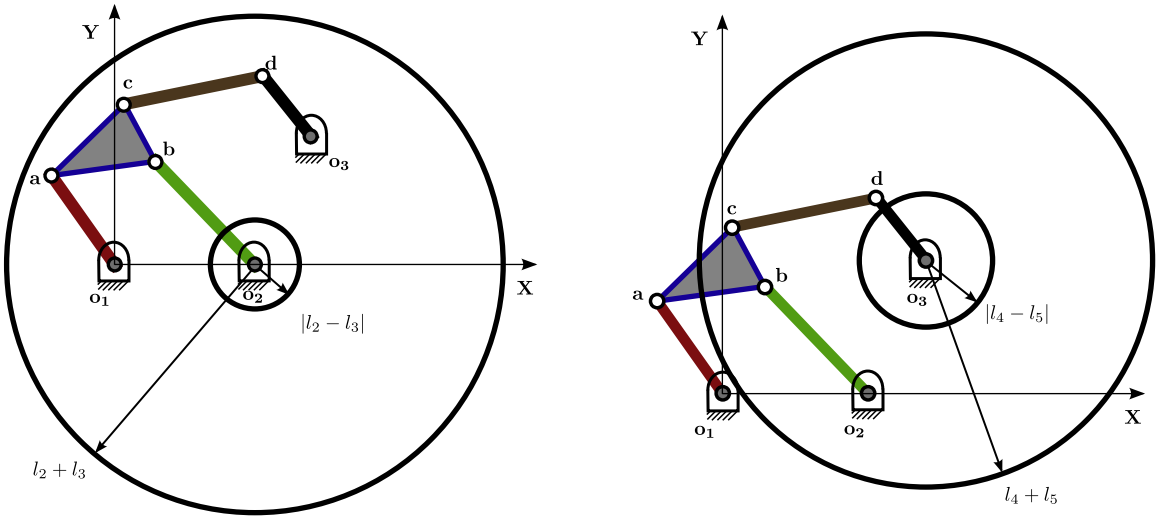

(a) The two concentric circles, centred at $\mathbf{o}_2$ and of radii l_2+l_3 and $|l_2-l_3|$, respectively, define the boundaries of the feasible region of the four-bar loop. The point **a** lies inside the annulus formed by the two circles.

(b) The two concentric circles, centred at $\mathbf{o}_3$ and of radii l_4+l_5 and $|l_4-l_5|$, respectively, bound the feasible region of the RR chain. The point **c** lies inside the annulus formed by the two circles.

Fig. 6. The geometric representation of the assembly conditions of the Stephenson-III mechanism.

In order to analyse the conditions for the polynomials to be positive, as required by Eq. (44), it may be noted that: a quartic polynomial, $p_0t_1^4+p_1t_1^3+p_2t_1^2+p_3t_1+p_4$, is positive $\forall t_1\in\mathbb{R}$, *iff* it does not have any real root and the coefficient of the highest degree term is positive. Thus, the conditions can be written as:

$$\begin{aligned}
&p_0>0, \quad \text{and}\\
&(P>0 \quad \vee \quad D>0) \quad \text{and}\\
&\Delta\geq 0, \quad \text{where}\\
&P=8p_0p_2-3p_1^2;\\
&D=64p_0^3p_4-16p_0^2p_2^2+16p_0p_1^2p_2-16p_0^2p_1p_3-3p_1^4.
\end{aligned} \tag{46}$$

In Eq. (46), Δ denotes the discriminant of the polynomial (see, e.g., [18] for the expressions and derivations). Hence, the mobility conditions can be written as:

$$\mathcal{M}_3 := \begin{cases} \mathcal{M}_{3a} := f_{3a} > 0, \\ \mathcal{M}_{3b} := f_{3b} > 0; \end{cases} \tag{47}$$

$$\mathcal{M}_4 := \begin{cases} \mathcal{M}_{4a} := f_{4a} > 0, \\ \mathcal{M}_{4b} := f_{4b} > 0. \end{cases} \tag{48}$$

As stated for the mobility functions $\mathcal{M}_1$ and $\mathcal{M}_2$, the functions $\mathcal{M}_3$ and $\mathcal{M}_4$ depend only on the architecture parameters, and it is required that the values of these functions are greater than zero for non-singular feasible mechanisms.

3.2. Mobility criteria for the Stephenson-III mechanism

As in the case of the Watt-II mechanism, the four-bar loop $\mathbf{o}_1\mathbf{abo}_2\mathbf{o}_1$ can be assembled *iff* $\forall\theta_1\in\mathbb{R}$, the distance $\overline{\mathbf{ao}_2}\in[|l_2-l_3|, l_2+l_3]$ (see Fig. 6), leading to the following conditions:

$$\mathcal{F}_1 := -l_0^2-l_1^2+2l_0l_1\cos\theta_1+(l_2-l_3)^2+\epsilon_1=0, \quad \epsilon_1\geq 0; \tag{49}$$

$$\mathcal{F}_2 := \quad l_0^2+l_1^2-2l_0l_1\cos\theta_1-(l_2+l_3)^2+\epsilon_2=0, \quad \epsilon_2\geq 0. \tag{50}$$

Similarly, the loop $\mathbf{o}_1\mathbf{acdo}_3\mathbf{o}_1$ can be assembled *iff* $\forall\theta_1\in\mathbb{R}$, the distance $\overline{\mathbf{co}_3}\in[|l_4-l_5|, l_4+l_5]$:

$$(x-o_{3x})^2+(y-o_{3y})^2\geq(l_4-l_5)^2, \tag{51}$$

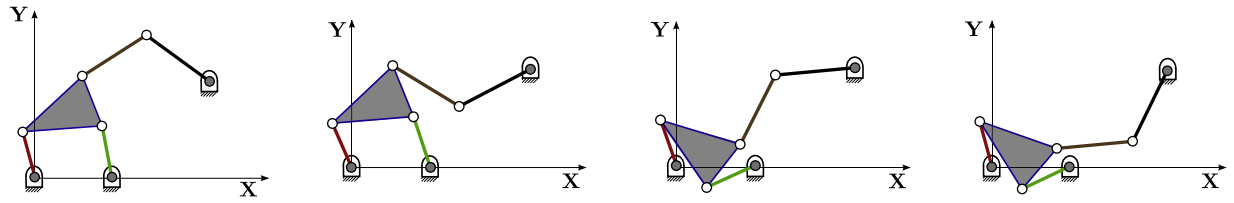

(a) UU: $s_1 < 0,\ s_2 < 0$ (b) UD: $s_1 < 0,\ s_2 > 0$ (c) DU: $s_1 > 0,\ s_2 < 0$ (d) DD: $s_1 > 0,\ s_2 > 0$

Fig. 7. The four branches of the Stephenson-III mechanism.

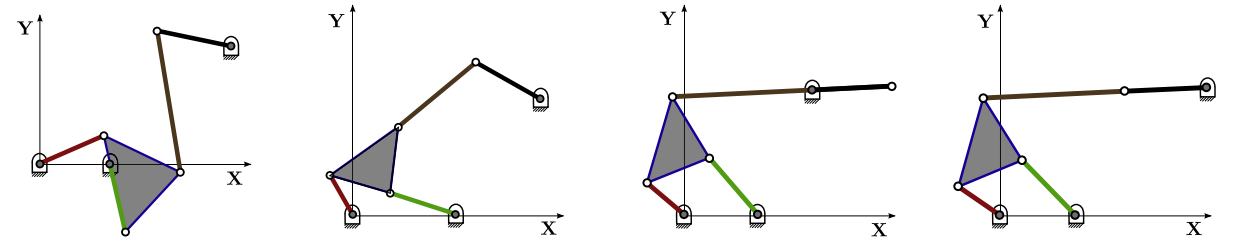

(a) Singularity in four-bar loop: $\phi_3 = \phi_2,\ \mathcal{S}_1 = 0$ (b) Singularity in four-bar loop: $\phi_3 = \phi_2 - \pi,\ \mathcal{S}_2 = 0$ (c) Singularity in RR chain: $\phi_5 = \phi_4,\ \mathcal{S}_3 = 0$ (d) Singularity in RR chain: $\phi_5 = \phi_4 - \pi,\ \mathcal{S}_4 = 0$

Fig. 8. The geometric representation of the four singularity conditions of the Stephenson-III mechanism. These conditions are mathematically equivalent to vanishing of the singularity functions $\mathcal{S}_1$, $\mathcal{S}_2$, $\mathcal{S}_3$ and $\mathcal{S}_4$, respectively.

$$(x - o_{3x})^2 + (y - o_{3y})^2 \leq (l_4 + l_5)^2, \tag{52}$$

where, $x = l_1 \cos\theta_1 + x_c \cos\phi_2 - y_c \sin\phi_2$, and $y = l_1 \sin\theta_1 + x_c \sin\phi_2 + y_c \cos\phi_2$ (see Fig. 2). The annular region, bounded by the two concentric circles centred at $\mathbf{o}_3$ and of radii $|l_4 - l_5|$ and $l_4 + l_5$, respectively, define the feasible locations of the coupler point **c**. The inequalities in Eqs. (51)and (52) are converted to equations using the slack variables ϵ_3 and ϵ_4:

$$\mathcal{F}_3 := -(x - o_{3x})^2 - (y - o_{3y})^2 + (l_4 - l_5)^2 + \epsilon_3 = 0, \quad \epsilon_3 \geq 0; \tag{53}$$

$$\mathcal{F}_4 := \quad (x - o_{3x})^2 + (y - o_{3y})^2 - (l_4 + l_5)^2 + \epsilon_4 = 0, \quad \epsilon_4 \geq 0. \tag{54}$$

The singularity condition, obtained from the vanishing of the determinant of the matrix, $\mathbf{J}_{\boldsymbol{\eta\phi}}$, is identical to that obtained in (32), for the Watt-II mechanism. The four kinematic branches of the Stephenson-III mechanism are depicted in Fig. 7. Here, the first and the second letters in the branch name indicate the configurations of the chains $\mathbf{abo}_2$ and $\mathbf{cdo}_3$, respectively.

The singularity conditions for the four-bar loop $\mathbf{o}_1\mathbf{abo}_2\mathbf{o}_1$ are depicted in Fig. 8(a) and (b). The steps to obtain the singularity conditions, $\mathcal{S}_1$ and $\mathcal{S}_2$, in terms of the input angle, θ_1, are exactly same as in Eq. (37) for the Watt-II mechanism, and hence, are not reproduced here.

The singularity in the loop $\mathbf{o}_1\mathbf{acdo}_3\mathbf{o}_1$ is governed by the function s_2, and occurs when $\phi_5 = \phi_4$, or $\phi_4 - \pi$. This is geometrically equivalent to l_4 and l_5 being collinear, as depicted in Fig. 8(c) and (d), respectively. For the singularity condition $s_2 = 0$, the variable ϕ_5 is eliminated by substituting ϕ_5 into the original loop-closure equations, Eqs. (18) and (19), to obtain a new set of constraint equations describing the singularities:

(a) $\phi_5 = \phi_4 \Rightarrow \mathbf{e}_3(\phi_3, \phi_4) = (e_{31}, e_{32})^\top = \mathbf{0}$,
(b) $\phi_5 = \phi_4 - \pi \Rightarrow \mathbf{e}_4(\phi_3, \phi_4) = (e_{41}, e_{42})^\top = \mathbf{0}$.

The sequential elimination of ϕ_4 and ϕ_5 can be schematically represented as follows:

$$\begin{aligned}
&\left.\begin{matrix}\eta_3(\theta_1,\phi_2,\phi_4,\phi_5)=0\\ \eta_4(\theta_1,\phi_2,\phi_4,\phi_5)=0\end{matrix}\right) \xrightarrow{\phi_5=\phi_4} \left.\begin{matrix}e_{31}(\theta_1,\phi_2,\phi_4)=0\\ e_{32}(\theta_1,\phi_2,\phi_4)=0\end{matrix}\right) \xrightarrow{\times\phi_4} \mathcal{S}_3(\theta_1,\phi_2)=0;\\
&\left.\begin{matrix}\eta_3(\theta_1,\phi_2,\phi_4,\phi_5)=0\\ \eta_4(\theta_1,\phi_2,\phi_4,\phi_5)=0\end{matrix}\right) \xrightarrow{\phi_5=\phi_4-\pi} \left.\begin{matrix}e_{41}(\theta_1,\phi_2,\phi_4)=0\\ e_{42}(\theta_1,\phi_2,\phi_4)=0\end{matrix}\right) \xrightarrow{\times\phi_4} \mathcal{S}_4(\theta_1,\phi_2)=0.
\end{aligned} \tag{55}$$

As in the case of Watt-II mechanism, the singularity functions $\mathcal{S}_1$ and $\mathcal{S}_2$ correspond to the feasibility conditions $\mathcal{F}_1$ and $\mathcal{F}_2$ given in Eqs. (49) and (50), when ϵ_1 and ϵ_2 vanish, respectively. Consequently, the singularity functions $\mathcal{S}_3$ and $\mathcal{S}_4$ in

Eq. (55) correspond to the feasibility conditions $\mathcal{F}_3$ and $\mathcal{F}_4$ given in Eqs. (53) and (54), when ϵ_3 and ϵ_4 reduce to zero, respectively. Hence, as before, for the mechanism to possess mobility, i.e., be feasible and non-singular, $\mathcal{F}_i = 0,\ i = 1, \ldots, 4$ for some $\epsilon_i > 0,\ i = 1, \ldots, 4$.

Obviously, the four-bar loop $\mathbf{o_1abo_2o_1}$ has the same mobility conditions as the four-bar loop for the Watt-II mechanism (reproduced here only for the sake of completeness):

$$\mathcal{M}_1 := \begin{cases} \mathcal{M}_{1a} := l_0 + l_1 + l_3 - l_2 & >0, \\ \mathcal{M}_{1b} := l_0 + l_1 + l_2 - l_3 & >0, \\ \mathcal{M}_{1c} := (l_0 - l_1)^2 - (l_2 - l_3)^2 & >0; \end{cases} \tag{56}$$

$$\mathcal{M}_2 := \begin{cases} \mathcal{M}_{2a} := l_1 + l_2 + l_3 - l_0 & >0, \\ \mathcal{M}_{2b} := l_0 + l_2 + l_3 - l_1 & >0, \\ \mathcal{M}_{2c} := (l_2 + l_3)^2 - (l_0 + l_1)^2 & >0. \end{cases} \tag{57}$$

Eqs. (53) and (54) can be converted to polynomial equations in t_1 and ϵ_i using the function $g_1(\theta_1, \phi_2)$ given in (21) and tangent half-angle substitution:

$$\left.\begin{aligned} \mathcal{F}_3(\theta_1, \phi_2, \epsilon_3) = 0 \\ g_1(\theta_1, \phi_2) = 0 \end{aligned}\right) \xrightarrow{\times \phi_2} h_1(\theta_1, \epsilon_3) = 0 \xrightarrow{\theta_1 \to t_1} h_3(t_1, \epsilon_3) = 0;$$
$$\left.\begin{aligned} \mathcal{F}_4(\theta_1, \phi_2, \epsilon_4) = 0 \\ g_1(\theta_1, \phi_2) = 0 \end{aligned}\right) \xrightarrow{\times \phi_2} h_2(\theta_1, \epsilon_4) = 0 \xrightarrow{\theta_1 \to t_1} h_4(t_1, \epsilon_4) = 0. \tag{58}$$

The functions h_3 and h_4 are quadratic in ϵ_i: i.e., $h_i = A_i(t_1)\epsilon_i^2 + B_i(t_1)\epsilon_i + C_i(t_1),\ i = 3, 4$. As ϵ_i are required to be positive, the conditions for the roots to be real and positive are similar to those described in (44). However, in this case, the polynomials f_{ia}, f_{ib} and f_{ic} are of degrees 6, 6 and 12 in t_1, respectively. The function f_{ic} does not contribute further to the mobility conditions for the same reasons as in the case of the Watt-II mechanism.

In order to analyse the condition for a six-degree polynomial in t_1 to be positive $\forall t_1 \in \mathbb{R}$, it may be first observed that as $t_1 \to \infty$,

$$P_6(t_1) \to \begin{cases} \infty, & \text{if} \quad p_0 > 0, \\ -\infty, & \text{if} \quad p_0 < 0, \end{cases} \tag{59}$$

where $P_6(t_1) = p_0 t_1^6 + p_1 t_1^5 + p_2 t_1^4 + p_3 t_1^3 + p_4 t_1^2 + p_5 t_1 + p_6$.

For the case $p_0 < 0$, the polynomial is negative for some $t_1 \in \mathbb{R}$, hence it is required that $p_0 > 0$ for $P_6(t_1) > 0\ \forall t_1 \in \mathbb{R}$. Furthermore, it is required that the minima of the polynomial are also positive, i.e., $P_6(t_1^*) > 0\ \forall t_1^*$ such that $P_6'(t_1^*) = 0$.

These requirements lead to the mobility conditions:

$$\mathcal{M}_3 := \begin{cases} \mathcal{M}_{3a} := f_{3a} & >0, \\ \mathcal{M}_{3b} := f_{3b} & >0; \end{cases} \tag{60}$$

$$\mathcal{M}_4 := \begin{cases} \mathcal{M}_{4a} := f_{4a} & >0, \\ \mathcal{M}_{4b} := f_{4b} & >0. \end{cases} \tag{61}$$

As with the other mobility functions, $\mathcal{M}_3$ and $\mathcal{M}_4$ depend only on the architecture parameters, and it is required that the values of these functions are greater than zero for the mechanism to be feasible and free of singularities.

4. Range mobility and branch identification

A general function generation problem may be defined over a range of the input angle, i.e., $\theta_1 \in [\theta_a, \theta_b]$. The mobility conditions given in the Section 3 ensures singularity-free feasible mechanisms for all $\theta_1 \in [0, 2\pi]$. These may reduce the solution space when an application demands mobility only for a finite range of motion, i.e., the *range* of the input angle may be a subset of $[0, 2\pi]$. Moreover, the mobility conditions above ensure that all the branches are feasible and non-singular. In general, one might be interested in a particular branch of the mechanism. In this section, the mobility conditions for a finite range of motion is derived, and also the branches of the mechanism are identified—using the formulation in the previous section.

4.1. Four-bar chain

The mobility conditions of the four-bar chain are common for both types of six-bar mechanism considered. For the four-bar chain to be non-singular and feasible for $\theta_1 \in [\theta_a, \theta_b]$, the mobility margins, ϵ_1, ϵ_2 need to be positive over the said range only. The values of t_1 for which the mobility margins become zero can be obtained from Eqs. (39) and (40):

$$\epsilon_1(t_1) = t_1^2\left((l_0 + l_1)^2 - (l_2 - l_3)^2\right) + (l_0 - l_1)^2 - (l_2 - l_3)^2 = 0, \tag{62}$$

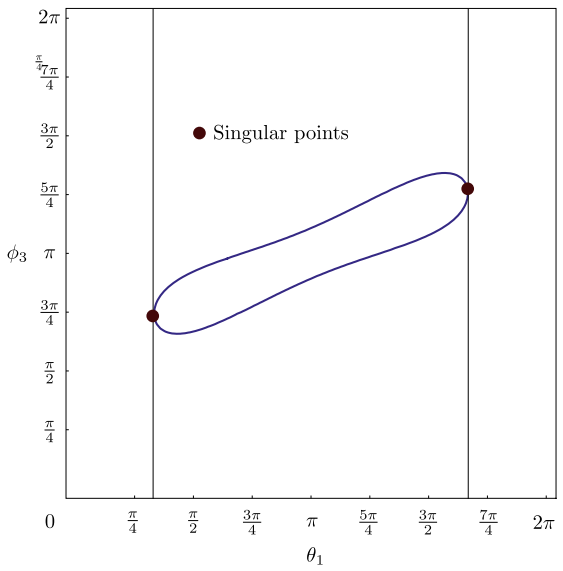

(a) Variation in the output angle, ϕ_3, with the change in θ_1. The solution branches merge at singular positions.

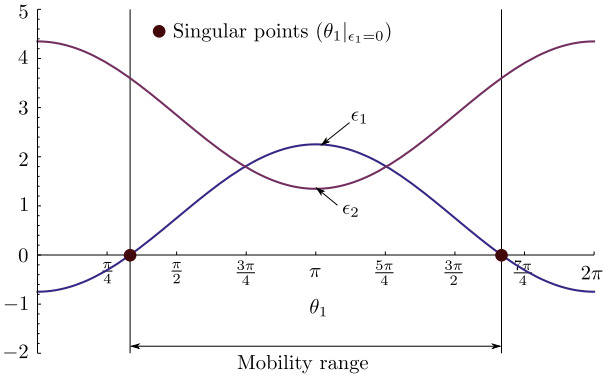

(b) Variation of the mobility margins, ϵ_1 and ϵ_2, with change in θ_1. At least one of the mobility margins vanishes at singular positions.

Fig. 9. The mobility of a four-bar mechanism over a specified range of values of input angle, θ_1, is determined by whether the mobility margins, ϵ_1 and ϵ_2, are positive over the range.

$$\epsilon_2(t_1) = t_1^2\left((l_2+l_3)^2 - (l_0+l_1)^2\right) - (l_0-l_1)^2 + (l_2+l_3)^2 = 0. \tag{63}$$

The corresponding real values of t_1 (and thereby of θ_1) for which $\epsilon_i = 0,\ i = 3, 4$, bound the range of the crank motion:

$$\theta_1|_{\epsilon_1=0} = \left\{\theta_1 \mid \epsilon_1\left(\tan\frac{\theta_1}{2}\right) = 0,\ \theta_1 \in \mathbb{R}\right\} \tag{64}$$

$$\theta_1|_{\epsilon_2=0} = \left\{\theta_1 \mid \epsilon_2\left(\tan\frac{\theta_1}{2}\right) = 0,\ \theta_1 \in \mathbb{R}\right\}. \tag{65}$$

The mobility margins, in terms of the input variable, θ_1, are obtained from Eqs. (25) and (26):

$$\epsilon_1(\theta_1) = l_0^2 + l_1^2 - 2l_0l_1\cos\theta_1 - (l_2-l_3)^2, \tag{66}$$

$$\epsilon_2(\theta_1) = -l_0^2 - l_1^2 + 2l_0l_1\cos\theta_1 + (l_2+l_3)^2. \tag{67}$$

The mobility condition over a finite range of input (which is less than a full-cycle) can be written as:

$$\mathcal{R}_i = \begin{cases} \epsilon_i(\theta_a) & >0 \\ \epsilon_i(\theta_b) & >0 \\ \theta_1 \notin [\theta_a, \theta_b] & \forall\theta_1 \in \theta_1|_{\epsilon_i=0} \end{cases} \qquad i = 1, 2. \tag{68}$$

The range mobility conditions are explained pictorially in the Fig. 9—the mechanism is non-singular and feasible only in the range where both the mobility margins are positive. The singular configurations are characterised by merging of the branches and also by the vanishing of one or both of the mobility margins. It should be noted that the mechanism becomes infeasible beyond the singularity, as at least one of the mobility margins become negative. Furthermore, the branches show similar characteristics in pair(s) , i.e., the two branches meet at a singularity and become infeasible thereafter together. The formulation also provides a means for finding the range over which the mobility conditions hold, rather than simply validating the mobility over a given range. However, the mechanism may have disjoint regions of mobility—a fact that needs to be incorporated in the implementation.

4.2. Watt-II mechanism

The mobility margins, ϵ_3 and ϵ_4, can be written as functions of ϕ_3 from Eqs. (29) and (30):

$$\epsilon_3(\phi_3) = 2l_a(l_0 - o_{3x})\cos(\alpha - \phi_3) + (l_0 - o_{3x})^2 + l_a^2 + 2l_a o_{3y}\sin(\alpha - \phi_3) + o_{3y}^2 - (l_4 - l_5)^2, \tag{69}$$

$$\epsilon_4(\phi_3) = -2l_a(l_0 - o_{3x})\cos(\alpha - \phi_3) - (l_0 - o_{3x})^2 + l_a^2 + 2l_a o_{3y}\sin(\alpha - \phi_3) - o_{3y}^2 + (l_4 + l_5)^2. \tag{70}$$

The steps for checking the mobility over a finite range of crank motion are detailed below.

1. Obtain the real values of θ_1, such that ϵ_3 or ϵ_4 is zero, from $h_3 = 0$ and $h_4 = 0$ given in (43):

$$\theta_1|_{\epsilon_3=0} = \left\{\theta_1 \mid f_{3b}\left(\tan\frac{\theta_1}{2}\right) = 0,\ \theta_1 \in [\theta_a, \theta_b]\right\}, \tag{71}$$

$$\theta_1|_{\epsilon_4=0} = \left\{\theta_1 \mid f_{4b}\left(\tan\frac{\theta_1}{2}\right) = 0,\ \theta_1 \in [\theta_a, \theta_b]\right\}. \tag{72}$$

2. It may be noted that the coefficients of the quadratic polynomials, defining the mobility margins, ϵ_3 and ϵ_4 (see Eqs. (43) and (44)), are themselves polynomials, and hence, *continuous* functions of the input angle. Therefore, their roots cannot change sign without passing through zero. Physically, this means that the mechanism cannot become *infeasible*, from a state of being feasible, without passing through a singularity. Hence, it is sufficient to check whether at least one of the roots of the polynomials vanishes inside the range of interest. Therefore, only the product of the roots, given by the functions f_{3b} and f_{4b} are considered.
   It is also important to check whether the relevant branch is affected, which leads to the steps mentioned below.
3. The values of ϕ_3 are calculated for all $\theta_1|_{\epsilon_3=0}$, $\theta_1|_{\epsilon_4=0}$ and $\{\theta_a, \theta_b\}$, corresponding to the desired branch, following the procedure described in Section 2.2 and given by the function $g_1(\theta_1, \phi_3)$ in Eq. (12). The branch can be identified using the signs of singularity functions, s_1 and s_2, given in Eqs. (33) and (34).
4. The mobility margins, ϵ_3 and ϵ_4, are evaluated from Eqs. (69) and (70), respectively. For the mechanism to be feasible and non-singular, these should be positive, leading to the conditions:

$$\mathcal{R}_k := \epsilon_k(\theta_1, \phi_3) > 0\ \forall\ \phi_3 \quad \text{s.t.}\ \ g_1(\theta_1, \phi_3) = 0,\ \text{ and } \theta_1 \in \{\theta_a, \theta_b\} \cup \theta_1|_{\epsilon_k=0}, \quad k = 3, 4. \tag{73}$$

5. The previous step is necessary to check whether the mobility margin is positive, as being free of singularity does not guarantee that the mechanism can be assembled.
6. The mobility margin serves as a measure of closeness of the mechanism to becoming infeasible. This has been illustrated in the example of the parabolic function generator described in Section 6.
7. It may be further observed that the range mobility conditions continue to be *closed-form* functions of the architecture parameters and do not involve any inaccuracies stemming out of any numerical computations.

4.3. The Stephenson-III mechanism

The mobility margins, ϵ_3 and ϵ_4, can be written as functions of ϕ_2 from Eqs. (53) and (54):

$$\epsilon_3 = (x - o_{3x})^2 + (y - o_{3y})^2 - (l_4 - l_5)^2, \tag{74}$$

$$\epsilon_4 = -(x - o_{3x})^2 - (y - o_{3y})^2 + (l_4 + l_5)^2. \tag{75}$$

The steps for checking the mobility over a finite range are detailed below.

1. Obtain the real values of θ_1, such that ϵ_3 or ϵ_4 is zero, from h_3 and h_4 given in Eq. (58):

$$\theta_1|_{\epsilon_3=0} = \{\theta_1 \mid f_{3b}\left(\tan\frac{\theta_1}{2}\right),\ \theta_1 \in [\theta_a, \theta_b]\}, \tag{76}$$

$$\theta_1|_{\epsilon_4=0} = \{\theta_1 \mid f_{4b}\left(\tan\frac{\theta_1}{2}\right),\ \theta_1 \in [\theta_a, \theta_b]\}. \tag{77}$$

2. The values of ϕ_2 are calculated for all $\theta_1|_{\epsilon_3=0}$, $\theta_1|_{\epsilon_4=0}$ and $\{\theta_a, \theta_b\}$, corresponding to the desired branch, from the equation $g_1(\theta_1, \phi_2) = 0$ (see Eq. (21)). The branch can be identified using the signs of singularity conditions, s_1 and s_2.
3. The values of ϵ_3 and ϵ_4 are evaluated from Eqs. (74) and (75). For the mechanism to be feasible and non-singular, these values should be positive:

$$\mathcal{R}_k := \epsilon_k(\theta_1, \phi_2) > 0\ \forall\ \phi_2 \quad \text{s.t.}\ \ g_1(\theta_1, \phi_2) = 0,\ \text{ and } \theta_1 \in \{\theta_a, \theta_b\} \cup \theta_1|_{\epsilon_k=0}, \quad k = 3, 4. \tag{78}$$

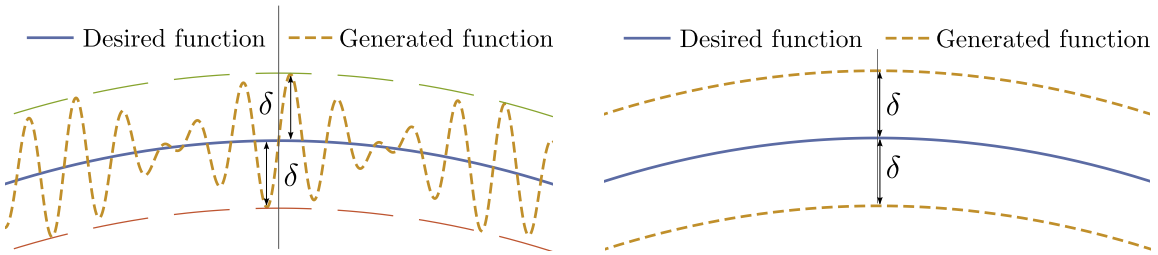

(a) Error function fluctuates within a bound of $\pm\delta$ about the desired value.

(b) Error is constant, at a value of δ, above/below the desired value.

Fig. 10. Types of errors in function generation and their implications.

5. Function generation using dual-order structural error

5.1. Definition of the dual-order structural error

For the Watt-II and the Stephenson-III mechanism, the function generation problem can be stated as:

$$\phi_5(\theta_1) = \phi_{5d}(\theta_1), \ \ \theta_1 \in [\theta_a, \theta_b], \tag{79}$$

where $\phi_{5d}(\theta_1)$ is the *desired* function, and $\phi_5(\theta_1)$ is the *actual* function *generated* by the mechanism, over $\theta_1 \in [\theta_a, \theta_b]$. This leads to the traditional definition of the *(zeroth-order) structural error* as:

$$\mathcal{E}_0(\theta_1) = \phi_5(\theta_1) - \phi_{5d}(\theta_1), \ \ \theta_1 \in [\theta_a, \theta_b]. \tag{80}$$

Minimisation of the maximum absolute value of the zeroth-order structural error (over the specified range of motion) leads to a mechanism in which this value is *bounded* by some upper limit. However, an objective considering only this aspect is *insensitive* to the variations of the error function within this bound. For instance, as shown in Fig. 10, both the cases (a) and (b) would lead to the same value of $\mathcal{E}_0$, whereas case (b) is clearly more desirable, since it would lead to lesser unwanted fluctuations in the output of the resulting mechanism. It is easy to see that the first-order error measure would be able to capture these fluctuations and mitigate them by reducing the variations in the error function. However, this measure, by itself, is insensitive to a constant error, however large. Therefore, it is logically appealing to use these measures of error *together*, in what may be termed as a *dual-order* formulation of the structural error. This has been done in the present work by means of a multi-objective formulation of the synthesis problem, in which each objective relates to the error in a distinct order. To the best of the knowledge of the authors, such a formulation is entirely novel.

The *first-order structural error* is defined as the derivative of the zeroth-order structural error:

$$\mathcal{E}_1(\theta_1) = \frac{d\mathcal{E}_0(\theta_1)}{d\theta_1} \tag{81}$$

$$= \frac{d\phi_5(\theta_1)}{d\theta_1} - \frac{d\phi_{5d}(\theta_1)}{d\theta_1} \tag{82}$$

$$= J_{\phi_5\theta_1}(\theta_1) - \frac{d\phi_{5d}(\theta_1)}{d\theta_1}, \ \ \theta_1 \in [\theta_a, \theta_b], \tag{83}$$

where $J_{\phi_5\theta_1}(\theta_1)$ is a velocity coefficient, defined in (22).

5.2. Design of function generators as an optimisation problem

An optimisation problem with constraints can be mathematically expressed as:

$$\begin{aligned} \text{Minimise} \quad & F_i(\mathbf{x}), \quad i = 1, 2, \ldots, p; \\ \text{subject to} \quad & G_j(\mathbf{x}) \geq 0, \quad j = 1, 2, \ldots, q; \\ & H_k(\mathbf{x}) = 0, \quad k = 1, 2, \ldots, r; \\ & x_l \in [a_l, b_l], \quad l = 1, 2, \ldots, w; \end{aligned} \tag{84}$$

where $F_i(\mathbf{x})$ are the objective functions, $\mathbf{x} = (x_1, \ldots, x_w)^\top$ is the vector of design variables, with x_l being bounded between a_l and b_l. The inequality and equality constraint functions are represented by $G_j(\mathbf{x})$ and $H_k(\mathbf{x})$, respectively. A maximisation problem can be converted to a minimisation problem by negating the appropriate objective(s).

The steps for posing the function generation problem as an optimisation problem are explained below.

1. The link dimensions of the mechanism are scaled with respect to one of the links, as the function generation problem is insensitive to the scale of the mechanism. In this paper, the link l_1 is assumed to have unit length, thereby reducing one dimension of the design space without affecting the generality of the solutions.
2. The input angle offset variable, θ_0, is incorporated into the formulation at this stage. The range of the function generation problem, say $\theta_f \in [\theta_a, \theta_b]$ (as shown in Fig. 6.1), changes to:

$$\theta_f = (\theta_1 - \theta_0) \in [\theta_a, \theta_b]. \tag{85}$$

3. For incorporating the output angle offset, ϕ_0, the desired output function to be generated, say $\phi_{5f}(\theta_f)$, is modified to:

$$\phi_{5d}(\theta_1) = \phi_{5f}(\theta_1 - \theta_0) + \phi_0. \tag{86}$$

4. The error functions are modified as given below:

$$\mathcal{E}_0(\theta_f) = \phi_5(\theta_1) - \phi_{5d}(\theta_1), \tag{87}$$

$$\mathcal{E}_1(\theta_f) = J_{\phi_5\theta_1}(\theta_1) - \frac{d\phi_{5d}(\theta_1)}{d\theta_1}, \tag{88}$$

where, $\theta_f = \theta_1 - \theta_0 \in [\theta_a, \theta_b]$.

5. A bi-objective optimisation problem is formulated. The first objective function is the maximum absolute zeroth-order error, i.e., $|\mathcal{E}_0(\theta_f)|$. The second objective function is given by the maximum absolute first-order error, i.e., $|\mathcal{E}_1(\theta_f)|$. The goal is to minimise these errors.
6. The mobility criteria, governed by the functions $\mathcal{M}_i,\ i = 1, \ldots, 4$ and $\mathcal{R}_i,\ i = 1, \ldots, 4$, described in Sections 3 and 4, form the constraints. For full-cycle mobility, the constraints given by $\mathcal{M}_i$ is used, whereas, for range mobility the constraints given by $\mathcal{R}_i$ are incorporated.
7. The objectives are computed by sampling the error functions at N uniformly-spaced discrete points in the range of interest of the input, N being decided based on a desired resolution. The number of sample points is decided based upon the resolution at which the error functions need to be evaluated. It may be noted that the mobility conditions are independent of the inputs and hence the sample size etc.
8. Roots of the FKU equation represent the solutions to the position kinematics for a given value of θ_1. The branches are distinguished on the basis of the sign of the singularity functions, as discussed in Section 3. A particular branch of interest is tracked for the function generation problem. The numerical optimisation is performed on each branch independently, thereby eliminating the possibility of the existence of branch-errors in the solutions obtained. This also ensures the exhaustive coverage of the potential solutions appearing in *all* the kinematic branches of the mechanism.

The dual-order function generation problem can be mathematically expressed as:

$$\begin{aligned} \text{Minimise:}\quad & F_1 := \max|\mathcal{E}_0(\theta_f)|, \\ & F_2 := \max|\mathcal{E}_1(\theta_f)|, \quad \text{where, } \theta_f \in [\theta_a, \theta_b]; \\ \text{subject to:}\quad & \mathcal{M}_k \quad \text{(for full cycle mobility)} \\ \text{or}\quad & \mathcal{R}_k \quad \text{(for range mobility)} \quad \text{where, } k = 1, \ldots, 4. \end{aligned} \tag{89}$$

6. Numerical examples

The above formulation of optimal design of the Watt-II and the Stephenson-III mechanisms for function generation is applied to a number of functions previously studied in literature:

1. A parabolic function, originally used by McLarnan in [19], and revisited in [3], generated using the Watt-II and the Stephenson-III mechanisms.
2. Range ballistic function as described in [20] and [3], generated using the Watt-II and the Stephenson-III mechanisms. The range ballistic function is used (in conjunction with elevation ballistic function) to find the orientation of guns to hit a target at a given distance and altitude.
3. Hip-motion generator as described in [5], generated using the Watt-II and the Stephenson-III mechanisms. The hip-motion generator is one of the three parts of a walking mechanism composed of six-bar mechanisms.
4. Double-dwell function given in [12], and used as a benchmark in [13], generated using the Stephenson-III mechanism. Double-dwell mechanisms are often preferred over cam-based mechanisms, the latter being prone to wear and more expensive [12].

The function generation problem is formulated as a multi-objective optimisation problem as explained in Section 5.2 and is solved using `NSGA-II` [16]. Few salient features of this algorithm, from a user's perspective, are:

1. The Genetic Algorithm (GA) is inspired by the natural process of evolution, wherein, a given *population* attempts to attain the optimal state, by improving over *generations*. These two parameters, i.e., the population size and the number of generations, are defined by the user, based on how the system tends to converge to the optimal solution(s).

Table 1
Bounds of the design variables in the parabola function generation problem ($x_l \in [a_l, b_l]$) for the Watt-II mechanism.

Variable (x_l)	l_0	l_2	l_3	l_4	l_5	α	l_a	o_{3x}	o_{3y}	θ_0	ϕ_0
Lower bound (a_l)	0.2	0.2	0.2	0.2	0.2	0	0.2	-20	-20	0	0
Upper bound (b_l)	6	6	6	6	6	2π	6	20	20	2π	2π

Table 2
Bounds of the design variables in the parabola function generation problem ($x_l \in [a_l, b_l]$) for the Stephenson-III mechanism.

Variable (x_l)	l_0	l_2	l_3	l_4	l_5	x_c	y_c	o_{3x}	o_{3y}	θ_0	ϕ_0
Lower bound (a_l)	0.2	0.2	0.2	0.2	0.2	-8	-8	-20	-20	0	0
Upper bound (b_l)	6	6	6	6	6	8	8	20	20	2π	2π

2. The initial population is randomly dispersed in the design space, the randomisation being seeded by a value input by the user.
3. The off-springs of the subsequent generations evolve, based upon *crossover* and *mutation*. The crossover operation produces children by considering the design vectors of a pair of parents in the current generation. The mutated children are created by imparting random modifications on a single individual of the current generation. The "good" solutions are used to create off-springs via crossover, thereby leading to convergence towards optimal solutions. The "bad" solutions are used to create mutated children, thereby leading to exploration. These operations are controlled by four parameters: (1) probability of crossover, (2) probability of mutation, (3) distribution index of crossover, and (4) distribution index of mutation. It has been observed that `NSGA-II` is sensitive to these parameters for certain problems. However, generic guidelines exist for appropriately choosing these control parameters [16].
4. For a multi-objective optimisation problem, generally, a set of optimal solutions is returned, as there may not be a single solution which is optimal from the perspective of all the objectives. The choice of a particular solution lies in the purview of the designer, which is often aided by the study of the *Pareto front* produced by `NSGA-II`.
5. While other optimisation techniques may be used, the authors have chosen GA as it is a global optimisation algorithm and does not require a "good" initial guess for the algorithm to converge. Moreover, `NSGA-II` has been widely used in solving optimisation problems and is found to be fairly robust, in such cases (see, e.g., [21,22]).

In the following, various desired output functions are described and the obtained results are documented.

6.1. Parabolic function

The parabolic function generation problem is specified in [3] as:

$$\phi_{5f}(\theta_f) = \frac{\theta_f^2}{90}, \ \forall \theta_f \in [0, 90^\circ], \quad \text{where all angles are in degrees.} \tag{90}$$

The function generation problem is formulated as described in Section 5.2. The maximum of the absolute value of the error functions, described in Eqs. (80) and (81), form the objective functions in the optimisation problem. The range mobility criteria, $\mathcal{R}_i, \ i = 1, \ldots, 4$, form the constraints. The problem is solved using both the Watt-II and the Stephenson-III mechanisms, using the bounds on the design variables[1], x_l, as given in Tables 1 and 2, respectively. In order to facilitate compactness and ease of fabrication of the mechanism, an additional constraint on the ratio of the link lengths is incorporated:

$$\rho = \max\{k_j\} / \min\{k_j\} \leq 6, \ \ j = 1, \ldots, 8, \tag{91}$$

where k_j comprise the parameters $l_i, \ i = 0, \ldots, 5$ and also the lengths of the three sides of the coupler link.

Two sets of optimisation runs are performed: (1) using the default numerical precision in `C++`, referred to as `binary64` by IEEE 754 standard, and, (2) after truncating the values of link lengths to three places after the decimal, and the angles truncated to two places. This is done to incorporate in the design process the fact that it may not be possible to manufacture links to beyond a certain accuracy level.

The objective functions are evaluated by sampling the desired range of motion. The number of sample points are taken to be $N = 400$, resulting in a resolution of 0.225° for the input angle, θ_1. The `NSGA-II` is run using a population of 2000, over 1000 generations, which takes nearly 10 min[2] of CPU time to cover all the branches of the mechanism. The `NSGA-II` parameters used for the optimisation runs, in all the examples, are detailed in Table 3. In order to accommodate the sensitivity of the results to these parameters, the probabilities of crossover and mutation are varied, within the ranges indicated.

[1] All linear dimensions are scaled with respect to the length of the input link, and hence, are unless. All angles are in radians, unless stated otherwise explicitly.

[2] Computational infrastructure: Intel Core i7-4770 CPU running at 3.40 GHz, with 32GB of RAM. The four kinematic branches are covered simultaneously in four different processes running in parallel, wherein each core solves the problem for one branch independently.

Table 3
`NSGA-II` parameters used in all the numerical optimisations reported in this paper.

Parameter name	Value
Population size	2000
Number of generations	1000
Probability of crossover	0.50–0.90
Probability of mutation	0.07–0.12
Distribution index of crossover	10
Distribution index of mutation	50
Seed for random number generator	0.5

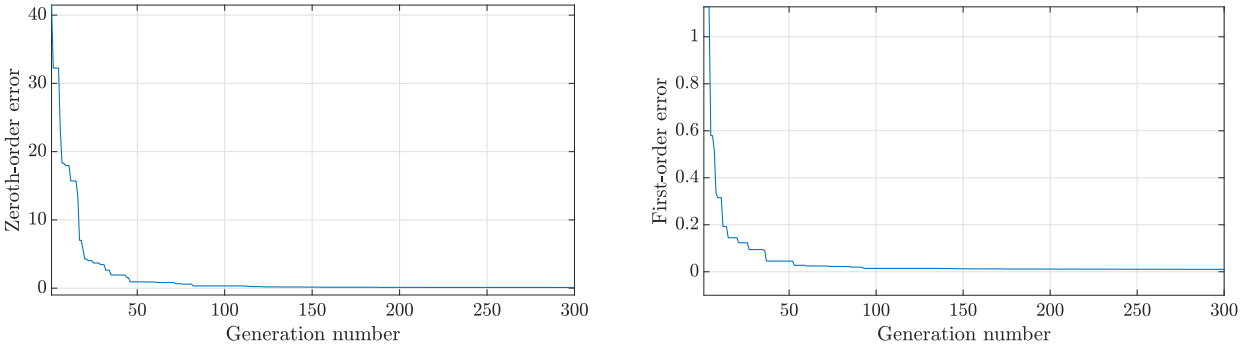

(a) Minimum zeroth-order error for each generation (b) Minimum first-order error for each generation

Fig. 11. Convergence of the two objective functions for the first 300 generations. The data is taken from the parabola function generation problem using the Watt-II mechanism.

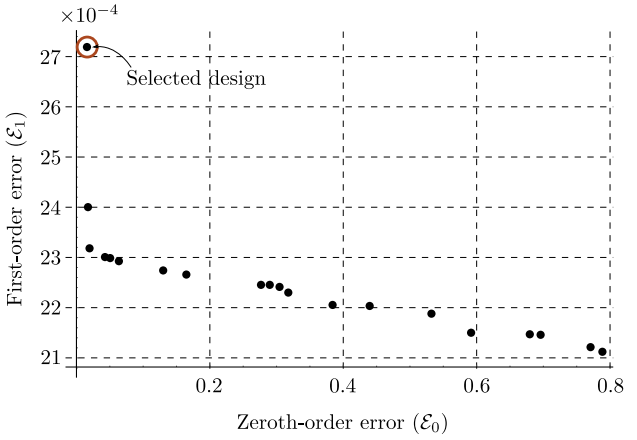

Fig. 12. Pareto front for parabola function generation using the Watt-II mechanism. The variation in the first-order error is of the order 10^{-3} and hence, is very small. The design is selected based on the minimum zeroth-order error.

The variation of the zeroth-order and the first-order errors are plotted against the number of generations in Fig. 11. As seen in the both the plots, the errors converge adequately within 100 generations, though the optimisation runs are carried through to 1000 generations (of which only the first 300 are depicted in the plots) mainly out of academic interest, motivated by the fact that the computational expenses involved are nominal.[3] The values of the two objective functions, based on the final population, are plotted in the form of a two-dimensional *Pareto front* (see, e.g., [23]), shown in Fig. 12. The designer is free to choose the preferred solution based on the application and the relevant tolerance limits. For example, in case of the Watt-II mechanism, it may be observed from Fig. 12 that the variation of the first-order error is very small—of the order 10^{-3}. Hence, the final design is selected based on the minimum zeroth-order error. The solution with the minimum zeroth-order error appeared in the branch DD. This particular solution has been used in the numerical results tabulated below. The architecture parameters obtained have been reported in Tables 4 and 5 for the Watt-II and the Stephenson-III

[3] Similar trends are seen in the other examples, which are not detailed here due to space constraints.

Table 4
Results: architecture parameters for the parabola function generation using the Watt-II mechanism (DD branch).

l_0	2.496	α	349.50°
l_1	1	l_a	5.606
l_2	3.165	o_{3x}	4.252
l_3	1.071	o_{3y}	−1.207
l_4	4.733	θ_0	154.70°
l_5	1.997	ϕ_0	286.48°

Table 5
Results: architecture parameters for parabola function generation using the Stephenson-III mechanism (UD branch).

l_0	4.731	x_c	2.797
l_1	1	y_c	-4.253
l_2	1.022	o_{3x}	0.451
l_3	5.407	o_{3y}	1.303
l_4	4.840	θ_0	180.48°
l_5	3.835	ϕ_0	74.48°

Table 6
Results and comparison with [3] for parabolic function using the Watt-II mechanism.

Error	Present work ($\rho \leq 6$)		From [3]
	Truncated	`binary64`	300 decimal
$\max \lvert\mathcal{E}_0(\theta_1)\rvert$	0.015	0.010	0.015
$\max \lvert\mathcal{E}_1(\theta_1)\rvert$	0.003	0.002	Data not available

Table 7
Results and comparison with [3] for parabolic function using the Stephenson-III mechanism.

Error	Present work ($\rho \leq 6$)		From [10]	From [3]
	Truncated	`binary64`		300 decimal
$\max \lvert\mathcal{E}_0(\theta_1)\rvert$	0.019	0.011	0.042	0.025
$\max \lvert\mathcal{E}_1(\theta_1)\rvert$	0.003	0.002	0.023	Data not available

mechanisms, respectively. The errors are reported and compared with [3] in Table 6 for the Watt-II mechanism and Table 7 for the Stephenson-III mechanism. Figs. 6.1 and 6.1 show the corresponding mechanisms for parabola function generation. The desired function, the generated function, and the dual-order errors are shown in Figs. 13 and 14. The plots of the output angles and the mobility margins are given in Fig. 15. The plots show the relation between the vanishing of the mobility margins and the mobility of the mechanism.

6.2. Range ballistic function

The range ballistic function is described in [20] and reformulated in [3]:

$$\phi_{5f}(\theta_f) = 45^\circ - \frac{1}{2}\arccos\left(-\frac{g}{v_0^2}\left(\frac{(25484.2-4000)\theta_f}{225}+4000\right)\right), \tag{92}$$

where $v_0 = 50$ m/s is the muzzle velocity of the artillery round, and g is the acceleration due to gravity, taken to be 9.81 m/s^2. All the angles are in degrees. It is assumed that there is no air resistance, and therefore the path of the projectile is parabolic.

The architecture parameters for the Watt-II are given in Table 8, and the errors are tabulated in Table 10.

Similarly, for the Stephenson-III mechanism the architecture parameters are given in Table 9, and the errors are given in Table 11. The mechanism and the error plots are not shown in either case, due to space constraint.

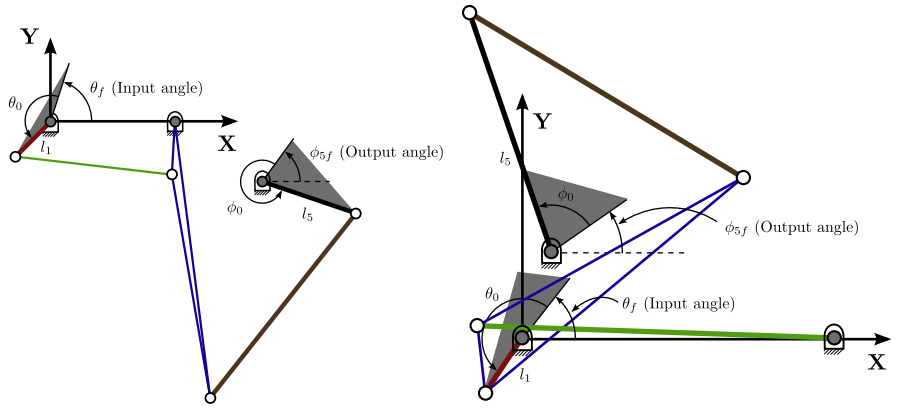

(a) The Watt-II mechanism for parabola function generation, as per Table 4.

(b) The Stephenson-III mechanism for parabola function generation, as per Table 5.

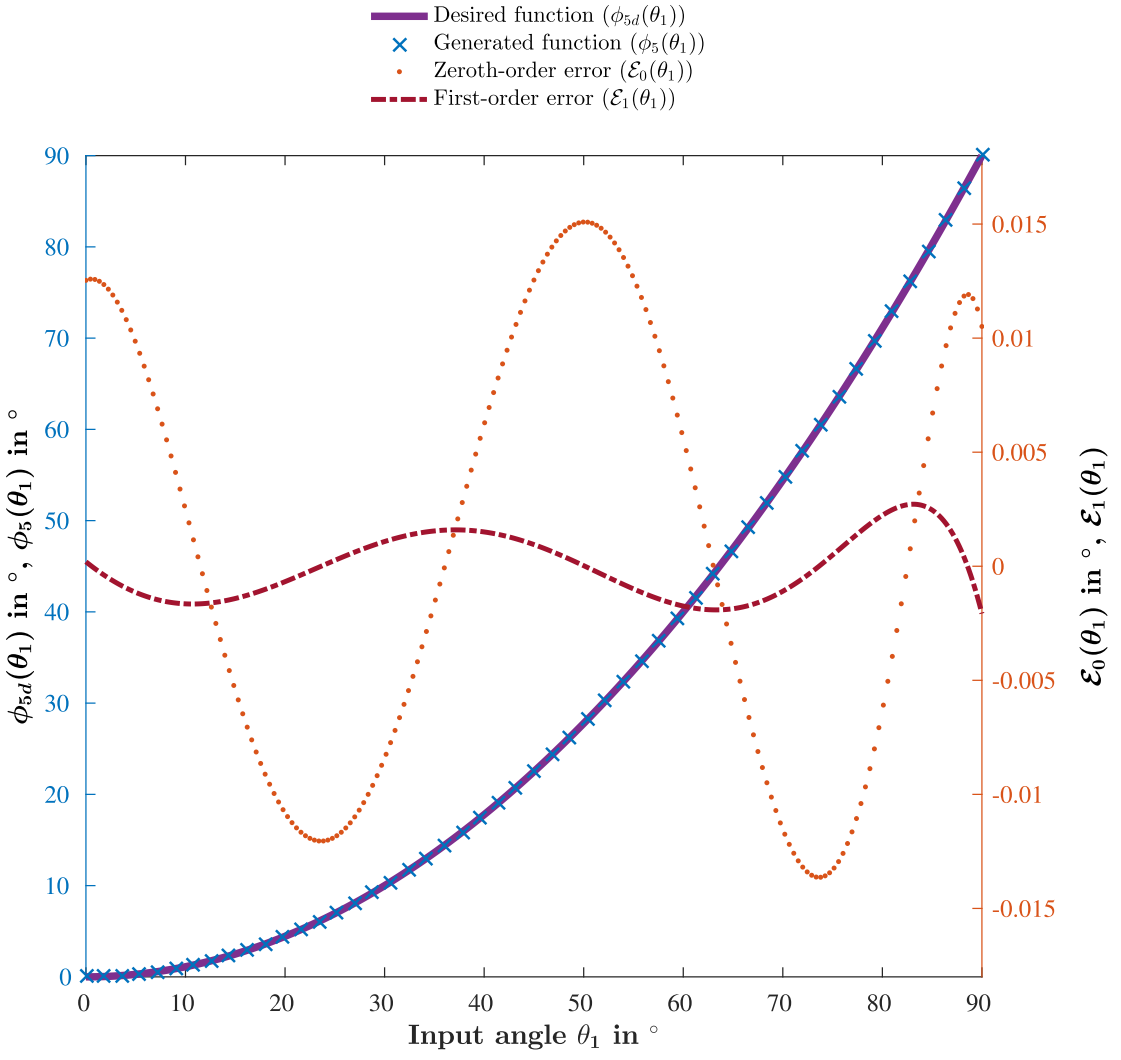

Fig. 13. The desired function, generated function, and errors in zeroth and first order for parabola function generation using the Watt-II mechanism.

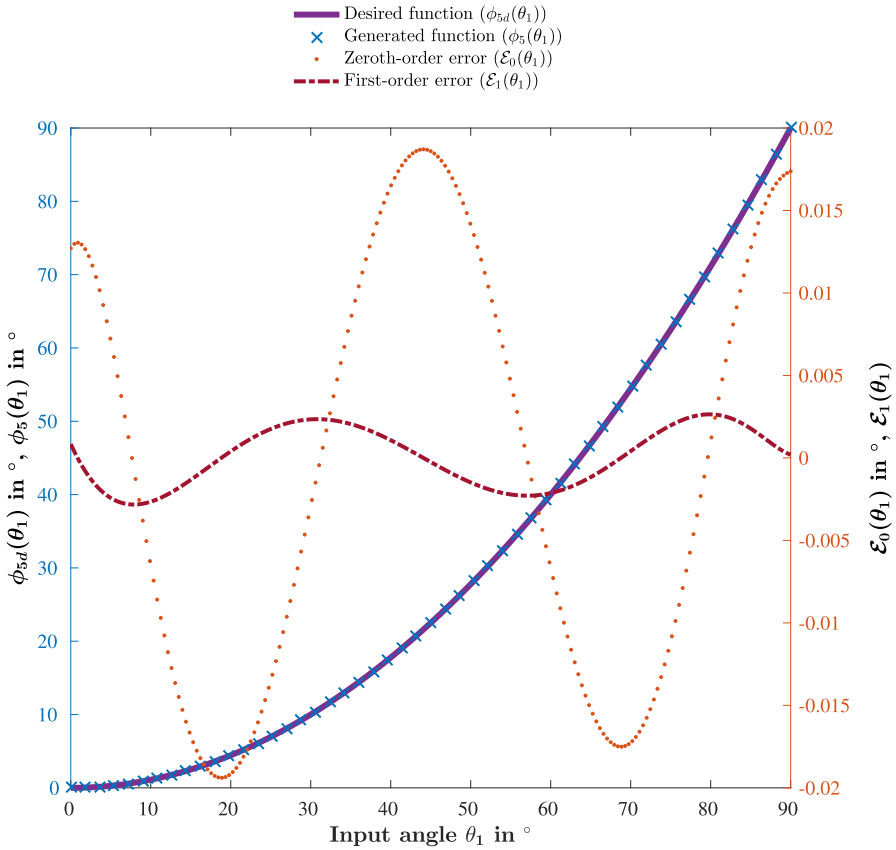

Fig. 14. The desired function, generated function, and errors in zeroth and first order for parabola function generation using the Stephenson-III mechanism.

Table 8
Results: architecture parameters for range ballistic function generation using the Watt-II mechanism (DD branch).

l_0	1.289	α	195.38°
l_1	1	l_a	2.789
l_2	2.513	o_{3x}	5.621
l_3	2.179	o_{3y}	−0.398
l_4	3.810	θ_0	125.48°
l_5	5.878	ϕ_0	163.87°

Table 9
Results: architecture parameters for range ballistic function generation using the Stephenson-III mechanism (DD branch).

l_0	2.371	x_c	4.156
l_1	1	y_c	2.558
l_2	4.850	o_{3x}	0.218
l_3	3.391	o_{3y}	−1.336
l_4	3.886	θ_0	115.74°
l_5	5.449	ϕ_0	37.82°

Table 10
Results for range ballistic function using the Watt-II mechanism.

Error	Present work ($\rho \leq 6$)	
	Truncated	`binary64`
$\max \lvert\mathcal{E}_0(\theta_1)\rvert$	0.135	0.130
$\max \lvert\mathcal{E}_1(\theta_1)\rvert$	0.124	0.101

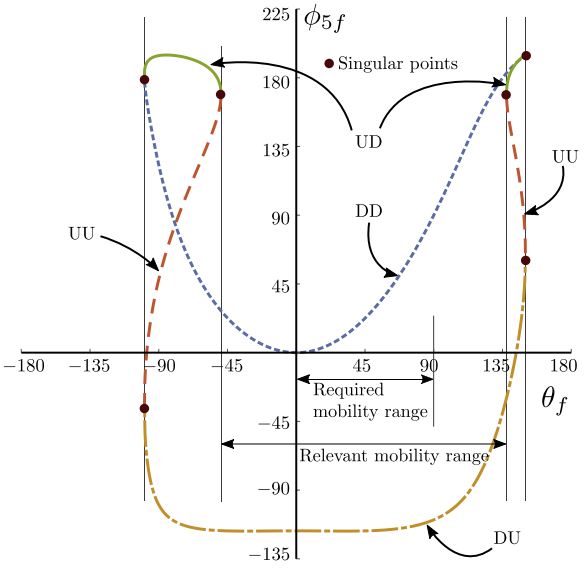

(a) Variation of the output angle, ϕ_{5f}, with the input angle, θ_f. All the four branches are shown. The branches merge at the singular points, denoted by the filled circles.

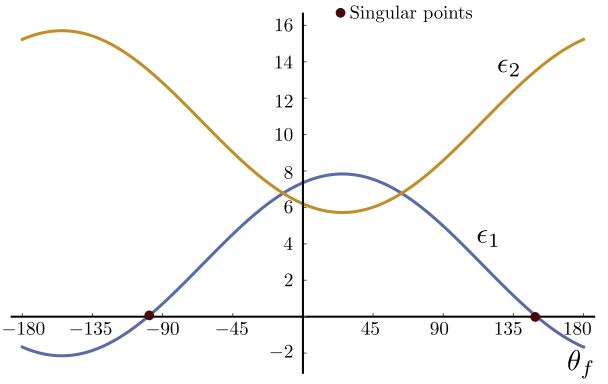

(b) The variation of the mobility margins corresponding to the four-bar loop, namely, ϵ_1 and ϵ_2. Singularity occurs when one or both mobility margin(s) vanish(es). The four-bar loop of the mechanism cannot be assembled once the either mobility margin becomes negative, hence there is no real solution for the output angle.

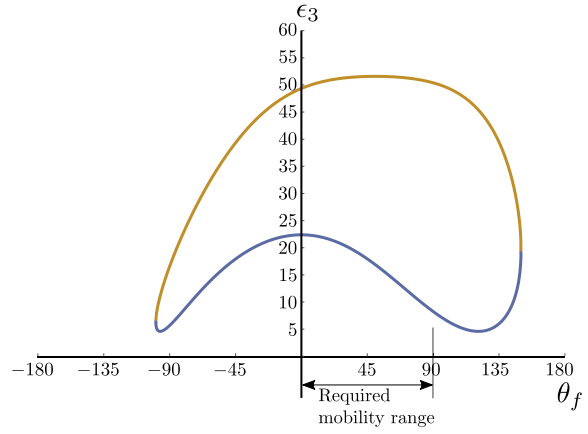

(c) The variation of the first mobility margin of the RR-chain, namely, ϵ_3. As it does not go to zero or negative, there is no affect on the mobility of the mechanism.

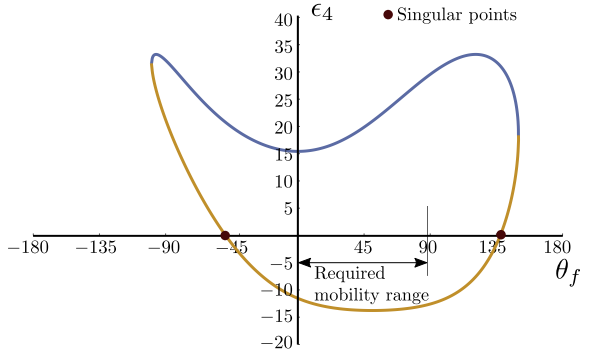

(d) The variation of the second mobility margin of the RR-chain, namely, ϵ_4. The value goes to zero and hence, limits the mobility range of the mechanism. As the mobility margin becomes negative, a pair of branches become infeasible, i.e., the mechanism cannot be assembled as per those branch configurations.

Fig. 15. The output angles and the mobility margins for the mechanism selected to generate parabola function using Watt-II mechanism. The figures portray the relation between the mobility margins and the mobility of the mechanism. As the mobility margin in the RR-chain, ϵ_4, goes to zero, a pair of branches merge together. This is in contrast with the singularity in the four-bar loop wherein both the pairs of branches merge.

Table 11
Results and comparison with [3] for range ballistic function using the Stephenson-III mechanism.

Error	Present work ($\rho \leq 6$)		From [3]
	Truncated	`binary64`	300 decimal
$\max \lvert\mathcal{E}_0(\theta_1)\rvert$	0.098	0.070	0.100 [a]
$\max \lvert\mathcal{E}_1(\theta_1)\rvert$	0.055	0.048	Data not available

[a] As read from Fig. 7 in [3].

Table 12
Fourier coefficients for hip motion function generation as specified in [5].

a_0	−0.23899606	a'_0	−0.12764964
a_1	0.26507432	b_1	0.04632108
a_2	0.00265777	b_2	0.05632819
a_3	−0.02058442	b_3	0.01472108

Table 13
Results: architecture parameters for hip motion generation using the Watt-II mechanism (DD branch).

l_0	2.608	α	294.50°
l_1	1	l_a	2.901
l_2	5.113	o_{3x}	8.160
l_3	3.678	o_{3y}	−4.560
l_4	2.727	θ_0	127.77°
l_5	5.252	ϕ_0	167.88°

Table 14
Results: architecture parameters for hip motion generation using the Stephenson-III mechanism (UD branch).

l_0	3.396	x_c	3.829
l_1	1	y_c	4.205
l_2	2.896	o_{3x}	−1.322
l_3	1.821	o_{3y}	11.894
l_4	2.786	θ_0	68.76°
l_5	4.824	ϕ_0	320.89°

6.3. Hip motion function

The hip motion function, as generated by a walking mechanism, proposed in [5], is a periodic function of time, t, described by the truncated Fourier series[4]:

$$f(t) = \frac{a_0}{2} + \sum_{m=1}^{3} (a_m \cos(mt) + b_m \sin(mt)) + a'_0. \tag{93}$$

The coefficients, a_m, b_m, are given in Table 12. The angular velocity of the input link is given to be 1 rad/s. Therefore, the function generation problem can finally be stated in terms of the input angle, θ_f, as:

$$\phi_{5f} = f(\theta_f), \tag{94}$$

where all angles are in radians. The hip motion is generated using both the Watt-II and the Stephenson-III mechanisms. The architecture parameters for the Watt-II mechanism are given in Table 13, and the errors are given in Table 15. Similarly, the architecture parameters for the Stephenson-III mechanism are given in Table 14, and the errors are given in Table 16.

6.4. Double-dwell function generation

The design of a six-bar mechanism having double-dwell at specified locations of the output link is a standard problem and has been studied in [12,13,24] recently using the optimisation approach. In this work, the double-dwell problem is

[4] In Eq. (95), a constant correction term, a'_0, had to be added in order to conform to the first row of Table 2 in [5]. The output function given in Eq.(33) of [5], as it is, does not agree with the table.

Table 15
Results for hip motion function using the Watt-II mechanism.

Error	Present work ($\rho \leq 6$)	
	Truncated	`binary64`
$\max\|\mathcal{E}_0(\theta_1)\|$	0.656	0.591
$\max\|\mathcal{E}_1(\theta_1)\|$	0.410	0.382

Table 16
Results for hip motion function using the Stephenson-III mechanism.

Error	Present work ($\rho \leq 6$)	
	Truncated	`binary64`
$\max\|\mathcal{E}_0(\theta_1)\|$	0.186	0.182
$\max\|\mathcal{E}_1(\theta_1)\|$	0.014	0.014

Table 17
Results: architecture parameters for double-dwell function generation using the Stephenson-III mechanism (UD branch).

l_0	2.116	x_c	1.262
l_1	1	y_c	1.036
l_2	1.617	o_{3x}	5.368
l_3	1.870	o_{3y}	-0.026
l_4	5.208	θ_0	343.77°
l_5	1.965	ϕ_0	6.30°

posed as a function generation problem, described as follows:

$$\phi_{5f}(\theta_f) = \begin{cases} \phi_{5f} = \phi_{51} & \forall \theta_1 \in [-15^\circ, 15^\circ], \\ \phi_{5f} = \phi_{52} & \forall \theta_1 \in [160^\circ, 220^\circ], \end{cases} \tag{95}$$

where ϕ_{51} and ϕ_{52} are the desired dwell output angles. The span of θ_1 is divided into $N_1 = 100$ and $N_2 = 400$ sample points for the first and the second dwell periods, respectively. The desired values of ϕ_5 at the first and the second dwell are $\phi_{51} = 225^\circ$ and $\phi_{52} = 210^\circ$, respectively.

6.5. Summary of the numerical studies

The seven examples reported above demonstrate clearly the efficacy of the formulation and the solution method. Even when compared with the solutions obtained using an exact synthesis method, the results obtained in this work are better in all the cases, wherever data are available for comparison. It may be noted that all the examples ran within 10–12 min, using no more than 4 cores of a standard desktop PC—which is minuscule, when compared to the computational requirements of the exact method. Each core is used to scan one of the four kinematic branches in general. However, the designer can choose to search for a feasible mechanism in any one, two, or three of the four branches, if needed.

The above results are enabled by two key novel theoretical developments, namely, the derivation of the mobility criteria of the mechanisms, explicitly in terms of link lengths and fixed pivot locations; and the concept of dual order formulation of the structural error. The first one helps confine the search for the optimal solution to the feasible region, thereby reducing the computation time very significantly, while the second helps in obtaining results of superior quality. The `NSGA-II` optimiser compliments the formulation very aptly. However, it may be noted that the burden of obtaining a good solution is not put entirely on the optimiser. The optimiser is used almost as a black-box tool, with all but two of the control/input parameters of the optimiser being kept fixed (see Table 3) across all the examples. Two of the parameters, namely, the probabilities of crossover and mutation, are varied over a 6×6 uniform grid overlaid on their respective ranges mentioned in the said table, and best result is reported. It is observed that all the 36 results in each example varied within the same order of magnitude, and hence the effect of finding the best set of `NSGA-II` control parameters leading to the best design results turned out to be an exercise of academic nature, than a functional one from a design standpoint. These studies show, that in principle, any other multi-objective optimiser could be used in conjunction with the proposed kinematic formulation of the problem(Fig. 16, Tables 17 and 18).

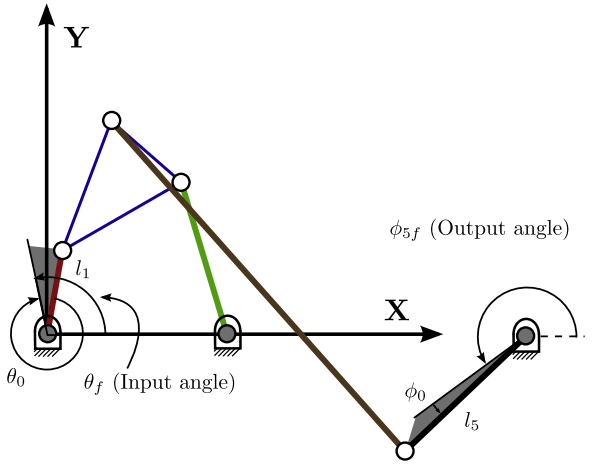

(a) The Stephenson-III mechanism for double dwell function generation, as per Table 17.

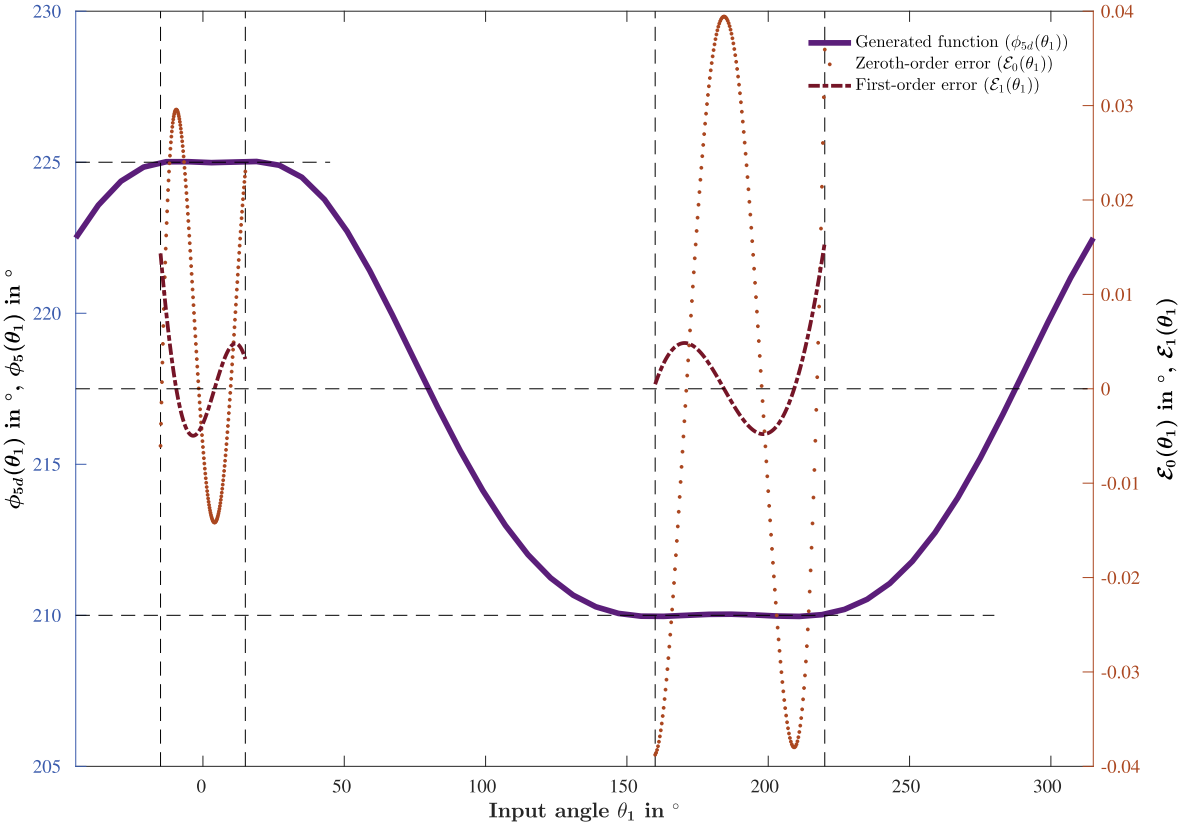

(b) The desired function, and errors in zeroth and first order for double dwell function generation using the Stephenson-III mechanism.

Fig. 16. Results for double dwell function generation using Stephenson-III mechanism.

Table 18
Results and comparison with [12] and [13] for double-dwell function generation.

Dwell Period	Error	Present work		[10]	[12]	[13][a]
		Truncated	`binary64`			
$\theta_1 \in [-15^\circ, 15^\circ]$	$\max \lvert\mathcal{E}_0(\theta_1)\rvert(\text{in}^\circ)$	0.029	0.024	0.049	0.556	0.044
$\phi_{51} = 225^\circ$	$\max(\lvert\mathcal{E}_1(\theta_1)\rvert)$	0.001	0.001	0.014	0.053	0.014
$\theta_1 \in [160^\circ, 220^\circ]$	$\max \lvert\mathcal{E}_0(\theta_1)\rvert(\text{in}^\circ)$	0.039	0.035	0.049	0.254	0.085
$\phi_{52} = 210^\circ$	$\max(\lvert\mathcal{E}_1(\theta_1)\rvert)$	0.001	0.001	0.018	0.031	0.006

[a] In [13] the first and the second dwell occur at $\phi_5 = 114.63^\circ$ and $\phi_5 = 125.28^\circ$, respectively. The zeroth order error is calculated as the difference between the maximum and the minimum values of the generated output in the respective ranges of the dwell motions in this case.

7. Conclusions

A new formulation for the optimal design of six-bar function generators has been presented in this paper. Several new concepts related to the mobility analysis, as well as the formulation of a multi-objective optimisation problem using the dual-order structural error have been introduced. The derivations and the corresponding results have been demonstrated via application to the Watt-II and the Stephenson-III mechanisms. To establish the efficacy of the proposed formulation, it has been bench marked against seven examples reported in the existing literature. In all of these, the results obtained in the proposed method exhibit improvements in terms of accuracy. The obtained results are free of branch errors, and conform to additional constraints on the range of link lengths. The CPU-time requirement associated with the formulation is very low, i.e., around 10–12 min on a standard desktop PC, as compared to the tens/hundreds of hours needed on 256/512 core computers necessary to implement the exact methods. The proposed formulation is applicable to other single-degree-of-freedommechanisms, including six-bar mechanisms of the other topologies. Analyses of these would be one of the future extensions of the present work.

References

[1] F. Freudenstein, An analytical approach to the design of four-link mechanisms, Trans. ASME 76 (1954) 483–492.
[2] S. Antonin, Mechanism for use in computing apparatus, 1943, US Patent 2,328,306.
[3] M.M. Plecnik, J.M. McCarthy, Numerical synthesis of six-bar linkages for mechanical computation, J. Mech. Rob. 6 (3) (2014) 031012.
[4] D. Bates, J. Hauenstein, A. Sommese, C. Wampler, Numerically Solving Polynomial Systems with Bertini, Software, Environments, and Tools, Soc. Ind. Appl. Math. (2013).
[5] M.M. Plecnik, J.M. McCarthy, Computational design of Stephenson-II six-bar function generators for 11 accuracy points, J. Mech. Rob. 8 (1) (2015) 011017.
[6] M.M. Plecnik, J.M. McCarthy, Kinematic synthesis of Stephenson-III six-bar function generators, Mech. Machine Theory 97 (2016) 112–126.
[7] S. Acharyya, M. Mandal, Performance of EAs for four-bar linkage synthesis, Mech. Mach. Theory 44 (9) (2009) 1784–1794.
[8] W.-Y. Lin, A GA-DE hybrid evolutionary algorithm for path synthesis of four-bar linkage, Mech. Mach. Theory 45 (8) (2010) 1096–1107.
[9] C.W. Wampler, A.P. Morgan, A.J. Sommese, Complete solution of the nine-point path synthesis problem for four-bar linkages, J. Mech. Des. 114 (1) (1992) 153–159.
[10] S. Agarwal, J. Badduri, S. Bandyopadhyay, Optimal synthesis of six-bar function generators, in: The 14th IFToMM World Congress, 2015, pp. 355–364.
[11] E. Sandgren, Design of single- and multiple-dwell six-link mechanisms through design optimization, Mech. Mach. Theory 20 (6) (1985) 483–490.
[12] P. Shiakolas, D. Koladiya, J. Kebrle, On the optimum synthesis of six-bar linkages using differential evolution and the geometric centroid of precision positions technique, Mech. Mach. Theory 40 (3) (2005) 319–335.
[13] M. Jagannath, S. Bandyopadhyay, A new approach towards the synthesis of six-bar double dwell mechanisms, in: A. Kecskeméthy, A. Müller (Eds.), Computational Kinematics, Springer Berlin Heidelberg, 2009, pp. 209–216.
[14] R. Srivatsan, S. Bandyopadhyay, Analysis of constraint equations and their singularities, in: J. Lenarčič, O. Khatib (Eds.), Advances in Robot Kinematics, Springer International Publishing, 2014, pp. 429–436.
[15] S. Bandyopadhyay, A. Ghosal, Analysis of configuration space singularities of closed-loop mechanisms and parallel manipulators, Mech. Mach. Theory 39 (5) (2004) 519–544.
[16] K. Deb, S. Agrawal, A. Pratap, T. Meyarivan, A fast and elitist multi-objective genetic algorithm: NSGA-II, IEEE Trans. Evol. Comput. 6 (2) (2002) 182–197.
[17] A. Ghosal, Robotics: Fundamental Concepts and Analysis, First ed., Oxford University Press, New Delhi, 2008.
[18] D. Lazard, Quantifier elimination: optimal solution for two classical examples, J. Symbolic Comput. 5 (1) (1988) 261–266.
[19] C.W. McLarnan, Synthesis of six-link plane mechanisms by numerical analysis, J. Manuf. Sci. Eng. 85 (1963) 5–10.
[20] A. Svoboda, Computing Mechanisms and Linkages, Dover publications, New York, 1965.
[21] A. Arikere, G.S. Kumar, S. Bandyopadhyay, Optimisation of double wishbone suspension system using multi-objective genetic algorithm, in: Asia-Pacific Conference on Simulated Evolution and Learning, Springer Berlin Heidelberg, 2010, pp. 445–454.
[22] J. Kilaru, M.K. Karnam, S. Agarwal, S. Bandyopadhyay, Optimal design of parallel manipulators based on their dynamic performance, in: Proceedings of the 14th IFToMM World Congress, 2015, pp. 406–412.
[23] K. Deb, Multi-Objective Optimization Using Evolutionary Algorithms, Wiley Interscience Series in Systems and Optimization, Wiley, 2001.
[24] R.R. Bulatović, S.R. Dordević, V.S. Dordević, Cuckoo search algorithm: a metaheuristic approach to solving the problem of optimum synthesis of a six-bar double dwell linkage, Mech. Mach. Theory 61 (2013) 1–13.